NASA Technical Memorandum 88250

IN-40201

An Experimental Investigation of Free-Tip Response to a Jet

Larry A. Young

September 1986

National Aeronautics and
Space Administration

NASA Technical Memorandum 88250

An Experimental Investigation of Free-Tip Response to a Jet

Larry A. Young, Ames Research Center, Moffett Field, California

September 1986

National Aeronautics and
Space Administration

Ames Research Center
Moffett Field, California 94035

NOMENCLATURE

A	tip transient response-curve integrated areas, rad-sec
b	tip forcing-frequency coefficient, nondim
C_A	free-tip aerodynamic damping coefficient, N-m-sec/rad
C_{A_n}	free-tip aerodynamic damping as a function of the nth harmonic component of the tip forcing frequency, N-m-sec/rad
CF	free-tip and controller-shaft mass centrifugal load, N
C_{ℓ_α}	tip lift coefficient curve slope, rad^{-1}
C_m	tip pitching-moment coefficient (nondim), positive noseup
C_{m_o}, C_{m_n}	steady-state and nth harmonic component of the tip aerodynamic pitching moment (nondim), positive noseup
C_{md_n}	unsteady nth-harmonic pitching-moment coefficient component that contributes to the tip aerodynamic damping, nondim
C_{ms_n}	unsteady nth-harmonic pitching-moment coefficient component that contributes to the tip aerodynamic spring, nondim
c_o	tip inboard-edge chord length, m
c_{pa}	tip pitch-axis location, % of chord
Δc	tip lift center offset from pitch axis, positive aft, m
e	blade lead-lag hinge offset, m
F	torsion-strap controller strap tensile load, N
F_n	Theodorsen function (nth harmonic)
G_n	second Theodorsen function (nth harmonic)
I	free-tip and controller-shaft polar moment of inertia, $kg\text{-}m^2$
k	tip-response reduced frequency, nondim
K	constant-moment controller spring constant, N-m/rad
K_A	free-tip aerodynamic spring constant, N-m/rad

K_{A_n}	free-tip aerodynamic spring as a function of the nth harmonic component of the tip forcing frequency, N-m/rad
$K_E = (K_A + K)$	equivalent-system spring constant, N-m/rad
ℓ	controller strap length, m
m	free-tip and controller-shaft mass, kg
M_c	controller moment output, N-m, positive noseup
M_d	tip moment due to aerodynamic damping, N-m, positive noseup
M_s	tip moment due to aerodynamic spring, N-m, positive noseup
MF	magnification factor, nondim
ΔP	air-jet plenum pressure, kPa
r	controller strap radius, m
r_f	tip forcing-frequency ratio, nondim
R	rotor radius, m
R_E	transient response envelope-area error estimate, nondim
R_m	free-tip and controller output shaft radial c.g. location, m
ΔR	tip span, m
t	total time interval of the free-tip transient response, sec
T_f	controller coulomb damping moment, N-m
v	tip downwash velocity, m/sec
V_T	tip speed, m/sec
W	weight of a free tip and controller shaft, N
β	blade flap angle, deg
δ	tip transient response logarithmic decrement, nondim
θ	free-tip pitch angle, deg, positive noseup
θ_n	nth harmonic of the free-tip pitching response, deg

θ_f	periodic forcing-function static displacement, deg
θ_{PT}	torsion-strap controller strap pretwist, deg, positive noseup
$\Delta\theta$	free-tip pitch angle with respect to inboard blade edge, deg, positive noseup
ϕ_s	controller strap slope, deg
Ω	rotor rotational speed, rad/sec
ω	tip natural frequency, rad/sec, or uncertainty analysis accuracy estimate
ω_d	tip damped-response frequency, rad/sec
ω_f	tip forcing-frequency, rad/sec
μ	controller bearing surface coefficient of friction, nondim
ρ	atmospheric density, kg/m^3
ψ	blade azimuth, deg
σ_E	regression analysis, standard-error estimate
τ	tip transient response period, sec
ζ	blade lead-lag angle, deg
ζ_d	free-tip damping ratio, nondim
ζ^*	free-tip/controller in-plane angle, deg

SUMMARY

The aerodynamic response of passively oscillating tips appended to a model helicopter rotor was investigated during a whirl test. Tip responsiveness was found to meet free-tip rotor requirements. Experimental and analytical estimates of the free-tip aerodynamic spring, mechanical spring, and aerodynamic damping were calculated and compared. The free tips were analytically demonstrated to be operating outside the tip resonant response region at full-scale tip speeds. Further, tip resonance was shown to be independent of tip speed, given the assumption that the tip forcing frequency is linearly dependent upon the rotor rotational speed.

INTRODUCTION

The free-tip rotor (FTR) is an innovative concept that has been proposed to meet two rotorcraft technology objectives: improve forward flight performance, and reduce rotor vibration loads. The FTR is similar to a conventional helicopter rotor for most of its span; however, the outboard 5-10% is allowed to pitch with respect to the inboard blade. Figure 1 shows a model FTR. Tip motion is constrained by a mechanically applied moment that forces the tip to passively seek a constant lift level. Figure 2 shows the free-tip concept. The mechanical device that generates the applied moment that the tip aerodynamic and inertial moments oppose is called the controller. The FTR controller applies a nonzero moment with a negligible mechanical-spring rate, so as to minimize the variation in tip lift.

Previous work published on the free-tip concept are references 1-10. Reference 1 is the patent taken out on the FTR conceptual predecessor, the constant lift rotor. References 2 and 3 are the original FTR performance analyses. References 4 and 5 contain the first FTR wind tunnel test data. Reference 6 is an early dynamic stability analysis of the FTR. References 7-10 are additional developmental studies of the FTR.

The first wind tunnel test of an FTR model revealed that its controller did not perform satisfactorily (refs. 4 and 5); there was almost no tip response to aerodynamic excitation. Therefore, the FTR concept could not be properly evaluated during the test. A development program was initiated to design and demonstrate a successful controller mechanism (ref. 9). Several candidate controller configurations were subjected to rigid plane rotation and evaluated, and a controller design was selected for the FTR. Since the success of the FTR concept was contingent upon the responsiveness of the tip and controller mechanism combination to aerodynamic excitation, it was necessary to whirl-test the complete system to verify

responsiveness. The response characteristics of the system demonstrated the readiness of the FTR for wind tunnel testing.

The purpose of this report is to present the results of the FTR whirl test. These results are in the form of tip transient-response measurements and empirical free-tip/controller spring and damping estimates. In addition to the experimental data presented, analytical expressions are derived for the free-tip aerodynamic spring, K_A, and aerodynamic damping, C_A. Comparisons are made between the analytical predictions and the experimental data.

DESCRIPTION OF APPARATUS

The model FTR used in this whirl test is the same model rotor used in the wind tunnel test described in references 4 and 5. The rotor modifications made for this test were a new controller and new tips that were increased from 5 to 10% span. The model dimensions are given in table 1. Figure 3 depicts the FTR model in the test chamber.

The free-tip controller design employed in this test is called the torsion-strap controller (TSC). The torque-output characteristics of the TSC mechanism are detailed in reference 9. The TSC derives its torque output from a twisted set of straps in tension, which is due to the centrifugal load of the tip mass, which is attached to the straps. The TSC design and the free-tip planform used in this test are shown in figure 4.

For the rotor whirl test, tip aerodynamic excitation was provided by an air jet normal to the tip-path plane. Therefore a tip angle-of-attack change occurred once per revolution, which initiated a free-tip pitch-angle, θ, transient response. The air jet was located at an azimuth station of approximately 180°. The jet could be raised and lowered by a hydraulic jack, and had an operating plenum-pressure range of $0 \leq \Delta P \leq 41$ kPa. The test-chamber corners were located at ψ = 45°, 135°, 225°, and 315°. The interference effects of the test-chamber corners were found to have significant effects on the free-tip responses.

A Hall-effect transducer measured the free tips' oscillations in response to the air jet, and was used to measure the pitch displacement, $\Delta\theta$, of the free tips with respect to the inboard blades. The transducer measured the magnetic flux of a magnet mounted on a free tip; as magnetic flux density is directly related to the distance from the magnet, the output voltage could therefore be calibrated for free-tip pitch-angle displacements. The response curves were sampled and averaged by a computer and reduced to Fourier coefficients.

FREE-TIP WHIRL-TEST RESULTS

The FTR concept requires the free tips to be highly responsive to aerodynamic forcing ($\omega >> 1/\text{rev}$) and to have a low controller spring constant relative to the aerodynamic spring ($K << K_A$). The purpose of the transient response data acquired during the whirl test was to verify that the free-tip/controller frequency and spring requirements were met. Additionally, analytical predictions of free-tip θ response have not been verified because of a lack of experimental data.

Before proceeding to the development of the experimental data-reduction algorithms and the free-tip aerodynamic theory necessary for data correlation and the verification of the tip/controller design response characteristics, it is appropriate to make a number of qualitative observations concerning free-tip θ time histories and FTR performance data acquired during the whirl test.

Free-Tip Time Histories

Free-tip θ time histories were measured by a Hall-effect transducer. Each time-history curve is the average of 20 tip time-history cycles. The individual θ time-history cycles were not retained by the data-acquisition system. All time histories were reduced by Fourier analysis to a set of experimental harmonic coefficients (summarized in table 2). A typical time history that includes the free-tip response to air-jet excitation is shown in figure 5.

Figures 6(a)-(c) are typical air-jet velocity distributions for various plenum pressures and displacements from the tip-path plane. The magnitude of the free-tip impulsive deflections from the steady-state pitch angle was dependent upon these two air-jet parameters. The air-jet velocity profile is assumed in the transient response data-reduction analysis to approximate a step-function excitation of the free tips.

Figure 7 is a transient response curve that has been digitally filtered to remove the steady state, the 1/rev, and on a conditional basis, the 2/rev harmonics of the tip pitch angle. The steady-state θ offset was removed to analyze the transient response. The 1/rev was eliminated to remove lateral and longitudinal cyclic influences on tip behavior. The 2/rev harmonic was sometimes filtered out according to a minimization of error strategy for the K_A and C_A coefficient regression. The 2/rev filtering was performed in an attempt to reduce the test chamber's corner-interference effects on the tip response data. Because a set of open windows were located along one wall of the test chamber, there was probably minimal aerodynamic interference from two of the test chamber's corners. For this reason the 2/rev was filtered out of the transient response data instead of the 4/rev. The initial deflection of the figure 7 transient response curve is located at a rotor azimuth position ($\psi \approx 190^\circ$) corresponding to the free tip exiting the air jet, where $\dot{\theta} \approx 0$.

The transient response of a free tip subjected to a step-function excitation should theoretically be the decaying sinusoid of a single degree of freedom, linear, combined coulomb and viscous underdamped system. A key reason for the nonlinear disagreement between the theoretical response and the experimental data may be the aerodynamic influence of the test chamber corners--in particular, the first corner after the air jet probably initiates a tip $\Delta\alpha$ change. The corner creates a recirculation zone that provides a localized upwash that interferes with tip response. It was therefore necessary, in developing data-reduction algorithms, to accommodate this response-curve distortion in the aerodynamic spring and damping calculations.

Whirl-Test Rotor Performance

During the FTR whirl test, rotor-performance data was acquired at very low C_T/σ. Figure 8 is a figure-of-merit curve, and figure 9 is a power-versus-thrust curve for the model FTR tested. Rigid-tip baseline information was not acquired. Low-thrust performance curves were obtained for two different controller pretwists (output moments) applied to the free tips. Rotor performance was not significantly affected by the free-tip control moment for the limited data set acquired.

FREE-TIP RESPONSE EXPERIMENTAL DATA-REDUCTION

To gain a complete understanding of the free-tip/controller response characteristics, it is necessary to determine values for the coefficients K, T_f, K_A, C_A, and I, which are, respectively, the controller mechanical spring and damping, the tip aerodynamic spring and damping, and the tip/controller polar moment of inertia. In the analytical results section, expressions will be derived for these response coefficients. In this section, data-reduction methods are developed that will later be used to calculate K, K_A, and C_A from experimental data for comparison with analytical predictions. Unfortunately, a satisfactory method for empirically determining T_f was not developed. The remaining coefficient, I, was estimated by simple analysis of the tip density distribution.

The mechanical spring, K, will be obtained from regression analysis of controller pull-test data. Three different methods will then be developed that attempt to estimate the aerodynamic spring and damping. All three data-reduction methods use the free-tip, air-jet response data to calculate K_A and C_A.

Controller Experimental Coefficients

Empirical estimates of the controller coulomb damping are unavailable. The data-reduction methods used could not satisfactorily isolate the T_f contribution from the total damping of the free-tip response curve.

Calibrations were performed on the controller that allowed an estimate of the spring constant to be made. Two check-load calibrations were made. First, a pull-test rig was assembled such that a tensile load (F = 7400 N, 100% rpm) could be applied to the TSC, while letting the strap angle be indexed through its allowable range. Second, the TSC controller was set to a specified angle (θ = 70°) and the strap tensile load was varied within its structural limits. The calibration curves are shown in figures 10(a) and 10(b).

The controller spring constant, K, can be estimated by these two curves by least-squares regression (ref. 9). The controller control moment can be represented by a semiempirical expression where the constant, A, is determined by regression analysis:

$$M_c = A\theta F$$

Therefore

$$K = AF = Am\Omega^2 R_m$$

An expression for A can be derived by noting the above M_c expression and equation (11) in the analytical-results section.

$$A = \frac{r^2}{\ell}$$

When the two controller calibrations were performed, it was noted that there was a 10% difference between the experimental estimate for A and the calculated analytical value. Experimentally, A was found to be 3.5×10^{-4} m, and the analytically derived A is equal to 3.9×10^{-4} m. Estimating the controller spring constant from the empirical value for A results in K = 2.59 N-m at V_T = 213 m/sec (800 rpm).

A typical analytically derived value of the aerodynamic spring is K_{A_n} = 53 N-m, as will be demonstrated in the analytical- and experimental-response comparison section. The subscript n denotes the number of the K_{A_n} harmonics used, which was 6. This choice of harmonic number will be explained in the experimental- and analytical-results correlation section. Therefore, with CF aligned with the controller straps, K contributes only approximately 5% of K_E.

It would be extremely difficult to isolate the actual K contribution to the K_E derived from the transient response data, because of the difficulty in defining the in-plane and out-of-plane free-tip/controller angular orientation. For although pull-test calibration data were obtained, the strap alignment with respect to the tip centrifugal force is not known and, as will be shown in the analytical-results section, a value for the controller spring constant cannot be estimated from the whirl-test data. Therefore, since the K values are relatively small, the experimental K_E estimates will be compared directly to analytical predictions of K_A.

Aerodynamic-Response-Coefficient Algorithms

Three data-reduction algorithms were developed to calculate the free-tip response coefficients from the experimental data. These algorithms were a logarithmic-decrement-averaging method, a differential-equation, least-squares-regression method, and a linear-decay-averaging method. Table 3 shows each method's coefficient-analysis capability. The differential-equation, least-squares regression approach is theoretically the most versatile of all the methods in that it should be capable of estimating all of the free-tip response coefficients. In comparison, the other two data-reduction methods were used to analyze the experimental data in terms of simplified models of the tip dynamic-pitching equation, resulting in a partial coefficient set. For example, the logarithmic decrement method assumes the tip response is only viscous damped, whereas the linear decay method assumes only coulomb damping.

The relative contributions of coulomb and viscous damping to free-tip damping is unknown because T_f cannot be experimentally determined. Further, using an analytical T_f prediction to determine the contribution of coulomb damping is impossible, as will be demonstrated in the analytical-results section. However, the accuracy of each of the above simplified models must be gaged by the accuracy of the curves generated from the coefficient estimates. For example, a poor comparison of an experimental θ time history with a response curve derived from a linear decay model would indicate that the tip/controller response is not predominately coulomb-damped.

The coefficient-regression results indicate that the logarithmic-decrement method is superior to the other two methods. Therefore, the free-tip/controller damping is predominately viscous. The logarithmic-decrement method will be discussed below. The remaining two methods will be discussed in Appendices A and B.

The logarithmic-decrement method is used to determine K_E and C_A. T_f cannot be estimated by this analysis. The method defines a "local" set of dynamic coefficients, based upon each cycle's amplitude decay, and estimates the tip-response coefficients by averaging all the local estimates. Equations (1) through (7) are the applicable equations for this method.

The transient response amplitude decay is represented by the parameter δ

$$\delta_i = \ln\left(\frac{\theta_j}{\theta_{j+1}}\right) \tag{1}$$

where θ_j and θ_{j+1} are the adjacent, transient, angular-displacement peaks for the jth and $(j+1)$th cycles. If the experimental response curve demonstrated no coulomb damping, nonlinear behavior, or data scatter, the parameter need be evaluated only once to estimate the system dynamic characteristics. However, to minimize the influence of these effects, the experimental data are evaluated for each cycle to obtain several δ estimates.

Next, given equation (1), reference 11 defines the damping ratio as

$$\zeta_{d_i} = \frac{\delta_i^2}{\sqrt{(2\pi)^2 + \delta_i^2}} \tag{2}$$

The remaining dynamic parameters can be determined from the following equations.

$$\omega_{d_i} = \frac{2\pi}{\tau_i} \tag{3}$$

where ω_d is the damped frequency, and τ_i is each cycle's damped-response period.

$$\omega_i = \frac{\omega_{d_i}}{\sqrt{1 - \zeta_{d_i}^2}} \tag{4}$$

The natural frequency, ω, is related to the damped frequency, ω_d, by means of the damping ratio.

Therefore, K_E and C_A are estimated locally to be

$$C_{A_i} = 2\zeta_{d_i} I\omega_i \tag{5}$$

and

$$K_{E_i} = I\omega_i^2 \tag{6}$$

where I is the free tip and the controller polar moment of inertia.

Finally, the effective response coefficients are assumed to be averages of the local, per cycle, coefficients.

$$C_A = \frac{1}{N}\sum_{i=1}^{N} C_{A_i}$$
$$K_E = \frac{1}{N}\sum_{i=1}^{N} K_{E_i} \tag{7}$$

Regression-Analysis Error Estimates

As was noted in the whirl-test results section, the free-tip time histories were digitally filtered prior to data-reduction. The steady-state and 1/rev harmonic terms were excluded from the Fourier series representing the tip transient responses. The 2/rev harmonic terms were sometimes also removed from the tip-response Fourier series. The 2/rev removal was performed in an attempt to reduce nonlinear distortions to the tip transient responses. These response distortions are not representative of the theoretical linear-response curves and are perhaps due to the interference effects from the test-chamber corners, of which were not successfully filtered completely out. Sets of coefficients were obtained from both versions of the transient response curve: one curve retaining the 2/rev, and the other with it removed. The results of both coefficient regression analyses were compared to the filtered experimental data and error estimates were calculated. The Fourier series, either with or without the 2/rev, which produced the smallest error estimate was assumed to have the more accurate coefficients. Therefore, the accuracy of the free-tip/controller spring and damping coefficients determined how much digital filtering was applied to the data.

Arriving at suitable error expressions was, therefore, an important data-reduction concern. The following section discusses the two error estimates that were used on the whirl-test free-tip data.

The first error estimate used on the whirl-test data was the standard error, which gave a point-by-point comparison of the experimental and curve-fit tip transient response. The second error estimate is concerned with free-tip gross-response behavior. It is perhaps more suitable as an exactness-of-fit measure than the standard error estimate, considering the test-chamber interference effects are not modeled, and therefore tend to invalidate a point-by-point comparison. This error estimate will be referred to as the envelope-area error estimate.

Using the envelope-area error measurement, a comparison is made between the experimental and curve-fitted response-curve envelopes. The assumption behind this error estimate is that equivalent envelope areas should indicate approximately equivalent envelope coordinates. Refer to figures 11(a)-(d). Figures 11(a) and 11(b) define the response-curve envelope and the envelope area respectively. Figures 11(c) and 11(d) demonstrate in principle an envelope-area comparison between the curve-fit response and the experimental response. While interference effects will negate a point-by-point correlation, their impact on parameter comparisons such as the envelope area should be less severe. The applicable equations for the envelope-area error estimate are shown below.

The experimental envelope area is approximated by a first order, trapezoidal-rule numerical integration.

$$A_{exp} = \sum_{i=1}^{N} \text{ABS}\ \frac{1}{2}\ (\theta_{i+1} - \theta_i)(t_{i+1} - t_i) \tag{8}$$

where θ_i and θ_{i+1} are adjacent experimental transient-peak amplitudes for each cycle, and t_i and t_{i+1} are the corresponding response times.

The curve-fit envelope area can be analytically estimated by integration of the exponential decay term in the underdamped-vibration general solution. This results in the expression

$$A_{calc} = \int_o^t \sqrt{1 - \zeta_d^2}\theta_o \, e^{-\zeta_d \omega t} \, dt$$

$$A_{calc} = -\frac{\sqrt{1 - \zeta_d^2}}{\zeta_d \omega} \theta_o [2e^{-\zeta_d \omega t} - T - 1] \tag{9}$$

where

$$T = e^{(-3\pi\zeta_d)/(2\sqrt{1-\zeta_d^2})}$$

Finally, a nondimensional parameter was derived that was used to compare not only the curve-fit results for a single test point, but also the results for other compatible test points. This parameter, R_E, eliminated the dependence of the error estimate on the free-tip initial deflection, which varied from one test point to another. Further, this particular parameter was used in weighted averages of the curve-fit coefficients. Coefficient weighting is appropriate in obtaining coefficient averages in that the relative accuracies of the regression analysis will differ significantly between data sets. The weighted averaging will be discussed in the analytical and experimental coefficient-comparison section. R_E is defined as

$$R_E = \frac{ABS(A_{exp} - A_{calc})}{A_{norm}} \tag{10}$$

where

$$A_{norm} = \theta_o t$$

is the normalizing scale, and t in equations (9) and (10) is the total time interval of the tip transient response.

FREE-TIP-RESPONSE ANALYTICAL RESULTS

A free tip is modeled as a single degree of freedom system with its controller and aerodynamic springs, and dampers, in parallel. In general, the free-tip response equation has the form

$$I\ddot{\theta} + C_A\dot{\theta} + (K_A - K)\theta + sgn(\dot{\theta})T_f = M(t)$$

where I is dependent upon the chordwise mass distribution of the tip and controller, C_A and K_A are dependent on the tip pitching-moment coefficient, K and T_f are functions of the controller kinematics and applied loads, and $M(t)$ is the time-dependent tip aerodynamic and centrifugal forcing moment. The function $\text{sgn}(\dot{\theta})$ returns the sign of $\dot{\theta}$.

The differential equation can be simplified by noting that there is no continuous external unsteady forcing being applied to the free tips during the whirl test (i.e., tip speed and the flap and lead-lag angle are all steady). The air jet does impose a 1/rev, short duration forcing of the tips, but for most of the rotor azimuth range, the tips are free of unsteady forcing. Therefore, the term $M(t)$ becomes negligible when the tips have exited the air jet, and the response equation becomes

$$I\ddot{\theta} + C_A\dot{\theta} + (K_A - K)\theta + \text{sgn}(\dot{\theta})T_f = 0$$

The objectives of the following analytical derivations are 1) obtain expressions for the dynamic parameters included in the whirl-test, free-tip response equation (i.e., C_A, K_A, K, and T_f); 2) demonstrate the validity of a simplification in the response equation that allows comparison between analytical predictions and experimental data (i.e., $K \ll K_A$ and $K_E \approx K_A$); 3) demonstrate analytically that the free-tip pitching motion is stable and nonresonant.

Derivation of Controller Response-Coefficients

The following linearized expression for the torque output of the TSC is presented in reference 9. The effect of flapping and lead-lag are not incorporated into the model.

$$M_c \approx \left(\frac{F}{\ell}\right) r^2(\theta_{PT} - \Delta\theta) \tag{11}$$

where F is equal to CF.

A TSC control-moment expression incorporating out-of-plane motion (flapping and lead-lag) will now be derived. The TSC derives its torque from a component of the strap tensile load, which is a component of the CF of the controller and tip mass. Since the controller out-of-plane motion will reduce the component of the CF acting through the TSC strap spanwise axis the torque output will also be reduced. Therefore, the condition for the maximum control moment occurs when $\beta = 0$ and $\zeta = 0$.

Refer to figure 12 for the freebody diagram of the effect of β and ζ on the tensile load. It can be seen that the strap tensile load, F, is expressed by

$$F = CF \cos\beta \cos\zeta^*$$

where

$$\zeta^* = \sin^{-1}\left[\frac{e}{R_m}\sin(180^0 - \zeta)\right]$$

Thus, equation (11) becomes

$$M_c \approx \left[m\Omega^2\left(\frac{R_m}{\ell}\right)r^2 \cos\beta\cos\zeta^*\right](\theta_{PT} - \Delta\theta)$$

which has the form

$$M_c \approx K(\theta_{PT} - \Delta\theta)$$

and so the controller spring is therefore

$$K = CF\cos\beta\cos\zeta^*\left(\frac{r^2}{\ell}\right) \qquad (12a)$$

A semi-empirical approach using equation (12a) and a check-load calibration is found to be necessary to accurately predict the TSC spring constant. This will be discussed in the analytical and experimental coefficient comparison section. The semiempirical estimate for K will confirm the relatively insignificant ($\approx$5% of K_A) contribution of K to K_E.

Another controller parameter that contributes to the dynamic (and static) behavior of a FTR free tip is the T_f term, the mechanism's friction-moment component. Reference 9 provides an expression for T_f for the special case of rigid-plane rotation:

$$T_f = \mu r\sqrt{(W\cos\beta + CF\sin\beta)^2 + (CF\sin\zeta^*)^2}$$

This expression incorporates β and ζ contributions to T_f. However, as a rigid rotating plane is assumed, the inertial loading on the controller bearings caused by the derivatives $d^2\beta/dt^2$ and $d^2\zeta^*/dt^2$ is not considered. An extension of the above T_f model will now be made to include the out-of-plane accelerations.

Figure 13 is a freebody diagram of the TSC showing its bearing contact forces, including inertial loads. In defining the inertial forces it is assumed that the tip and controller output shaft CG is located on the shaft axis. The inertial forces are additive to the steady-state bearing contact forces. Therefore, the modified friction equation becomes

$$T_f = \mu r\sqrt{\left(W\cos\beta + CF\sin\beta + mR_m\frac{d^2\beta}{dt^2}\right)^2 + \left(CF\sin\zeta^* + mR_m\frac{d^2\zeta^*}{dt^2}\right)^2} \qquad (12b)$$

The controller out-of-plane angular orientation and acceleration components are very difficult to determine. Additionally, μ is not easily determined. Therefore, the controller T_f could not be analytically predicted for the whirl-test case. A measurement of the controller friction coefficient and controller accelerations are required before an accurate T_f estimate can be made.

Derivation of Aerodynamic Damping Coefficient

In forward flight, the free tip is subjected to a periodic, external forcing function consisting of tip relative-velocity changes, varying local inflow, and blade flapping. A rotor in hover, or being whirled, is generally not subjected to a tip forcing-function. For the free-tip whirl-test, the tips are subjected to forcing once per revolution by sudden angle-of-attack changes caused by an air-jet blowing through the tip-path plane. Considered on a per cycle basis, the air-jet excitation approximates a step function input to the free-tip spring and damper system. Given the relative simplicity of the whirl-test free-tip forcing, it is possible to analytically derive C_A and K_A.

An analytical expression will now be derived for the aerodynamic damping coefficient for a whirl-tested free-tip. There are two important assumptions for the following aerodynamic damping and spring analysis: steady inflow and negligible periodic out-of-plane blade motion. For a rotor in hover, or being whirl-tested, these assumptions are valid.

Equation (13), derived in reference 3, describes the free-tip aerodynamic moment

$$M_A = \frac{1}{2} C_m c_o^2 \Delta R \rho (\Omega R)^2 \tag{13}$$

with the aerodynamic moment consisting of two components

$$M_A = M_S + M_d$$

where M_S is the moment due to aerodynamic spring, and M_d is the aerodynamic damping moment.

The contribution to M_A caused by damping is

$$M_d = \frac{1}{2} C_{md} c_o^2 \Delta R \rho (\Omega R)^2 \left(\frac{d\theta}{dt}\right) \tag{14}$$

where C_{md} incorporates all the terms of C_m that are constant multipliers of $d\theta/dt$.

Reference 10 demonstrates that C_m can be represented by a linear combination of harmonic components for unsteady flow about the free tip. Therefore, the damping moment contribution for each harmonic can be written as

$$M_{d_n} = \frac{1}{2}\rho c_o^2 \Delta R V_t^2 C_{md_n}\left(\frac{d\theta_n}{dt}\right) \tag{15}$$

where $V_t = \Omega R$ and the subscript n denotes the harmonic number.

Reference 10 derived equations (16(a)-(d)) for the harmonic components of C_m, for the two-dimensional (2-D) case. These equations are based on Theodorsen unsteady potential-flow analysis. It is necessary to apply corrections to the 2-D inviscid C_A and K_A predictions or they will significantly differ from the experimental spring and damping values. The possible corrections might be in the form of modifications to the 2-D, unsteady pitching-moment coefficient equations or substitution of new C_{ℓ_α} values obtained from computational fluid dynamic solutions or from experimental data. Data from a low-speed, wind-tunnel semi-span test with indexed tips was used to calculate C_{ℓ_α} values. The geometry of one of the tips studied during this test was the same as the whirl-test free tips. Therefore, an attempt to correct the damping predictions for the free tips was made by using these empirical tip semi-span values for C_{ℓ_α} in the 2-D, potential-flow C_m expression.

The steady-state pitching-moment coefficient is obtained from

$$C_{m_o} = C_{\ell_\alpha}\left\{\left(c_{pa} - \frac{1}{4}\right)\left[\vartheta_o + \frac{1}{V_t}v + c_o\left(\frac{3}{4} - c_{pa}\right)\frac{\Omega\beta_o}{V_t}\right] + \frac{c_o}{4}\left(c_{pa} - \frac{3}{4}\right)\frac{\Omega\beta_o}{V_t}\right\} \tag{16a}$$

The harmonic unsteady-moment coefficient is obtained from

$$\begin{aligned} C_{m_n} = C_{\ell_\alpha}\Bigg(&\left(c_{pa} - \frac{1}{4}\right)\left\{\left[F_n - c_o\left(\frac{3}{4} - c_{pa}\right)\frac{G_n n\Omega}{V_t}\right]\theta_n + \frac{G_n}{n\Omega V_t}\frac{dv}{dt} + \frac{F_n}{V_t}\frac{dv}{dt}\right. \\ &\left. + \left[c_o\left(\frac{3}{4} - c_{pa}\right)\frac{F_n}{V_t} + \frac{G_n}{n\Omega}\right]\left(\frac{d\theta_n}{dt} + \Omega\beta_n\right)\right\} + \frac{c_o}{4}\left\{\left(c_{pa} - \frac{3}{4}\right)\left(\frac{d\theta_n}{dt} + \Omega\beta_n\right)\frac{1}{V_t}\right. \\ &\left.\left. + \left(c_{pa} - \frac{1}{2}\right)\frac{dv}{dt}\frac{1}{V_t^2} - c_o\left[\frac{1}{32} + \left(c_{pa} - \frac{1}{2}\right)^2\right]\left(\frac{d^2\theta_n}{dt^2} + \Omega\frac{d\beta_n}{dt}\right)\frac{1}{V_t^2}\right\}\right) \end{aligned} \tag{16b}$$

where the reduced frequency, k, is

$$k = \frac{c_o n\Omega}{2V_t} = \frac{c_o n}{2R} \tag{16c}$$

and the functions, F_n and G_n, are defined by the complex Bessel-function expression

$$F + iG = \frac{J_1(k) - iY_1(k)}{J_1(k) + Y_o(k) - i[Y_1(k) - J_o(k)]} \tag{16d}$$

Damping coefficients are defined as constant multipliers to $d\theta_n/dt$. Therefore, the θ time-derivative coefficients are separated from the above equations (16a-d) and are incorporated into the C_{md} expression. And so

$$C_{md_n} = C_{\ell_\alpha}\left\{\left(c_{pa} - \frac{1}{4}\right)\left[c_o\left(\frac{3}{4} - c_{pa}\right)\frac{F_n}{V_t} + \frac{G_n}{n\Omega}\right] + \frac{c_o}{4V_t}\left(c_{pa} - \frac{3}{4}\right)\right\} \tag{17}$$

Equation (15) can be rearranged as

$$C_{A_n} = \frac{M_d}{d\theta_n/dt}$$

where

$$C_{A_n} = \frac{1}{2}\rho c_o^2\ \Delta R V_T^2 C_{md_n} \tag{18}$$

Substituting equation (17) into (18), and simplifying, results in the following relation

$$C_{A_n} = \frac{1}{2}\rho\ \Delta R C_{\ell_\alpha}\left[c_o^3\left(\frac{1}{4} - c_{pa}\right)\left(\frac{3}{4} - c_{pa}\right)F_n V_T + \frac{1}{n}c_o^2\left(\frac{1}{4} - c_{pa}\right)G_n R V_T + \frac{1}{4}c_o^3\left(\frac{3}{4} - c_{pa}\right)V_T\right] \tag{19}$$

All that remains to estimate the free-tip aerodynamic damping are the explicit expressions for both F_n and G_n. By manipulating equation (16d) and separating the real and imaginary terms into two relationships, the two functions are found to be

$$F_n = \frac{J_1(k)[J_1(k) + Y_o(k)] + Y_1(k)[Y_1(k) - J_o(k)]}{[J_1(k) + Y_o(k)]^2 + [Y_1(k) - J_o(k)]^2}$$

$$G_n = \frac{J_1(k)[Y_1(k) - J_o(k)] - Y_1(k)[J_1(k) + Y_o(k)]}{[Y_1(k) - J_o(k)]^2 + [J_1(k) + Y_o(k)]^2} \tag{20}$$

where $J_o(k)$, $J_1(k)$, $Y_o(k)$, and $Y_1(k)$ are Bessel functions of the first and second kind of order zero and one, dependent upon the reduced frequency, k.

Equations (16c), (19), and (20) describe a complete solution for C_{A_n}, the free-tip aerodynamic damping. An uncertainty analysis of the aerodynamic-damping

equations is included in Appendix C. The C_A predictions discussed in the analytical- and experimental-results comparison section will be accompanied by damping uncertainty estimates based upon the analysis in the appendix.

Derivation of Aerodynamic Spring Constant

Similarly, an equation for the aerodynamic spring can be estimated from coefficients taken from equations (16a-d), and substituted into equation (13).

$$M_s = \frac{1}{2} \rho c_o^2 \Delta R V_T^2 C_{ms_n} \theta_n$$

where C_{ms_n} incorporates terms from equations (16 a-d) that are constant multipliers of θ_n.

The spring is then

$$K_{A_n} = \frac{M_s}{\theta_n}$$

Or, therefore

$$K_{A_n} = \frac{1}{2} \rho c_o^2 \Delta R V_T^2 C_{ms_n} \tag{21}$$

Where from equation (16b)

$$C_{ms_n} = C_{\ell_\alpha} \left(c_{pa} - \frac{1}{4}\right) \left[F_n - c_o \left(\frac{3}{4} - c_{pa}\right) \frac{G_n n}{R}\right] \tag{22}$$

Substituting equation (22) into (21) results in

$$K_{A_n} = \frac{1}{2} \rho \Delta R V_T^2 c_o^2 \left(\frac{1}{4} - c_{pa}\right) \cdot C_{\ell_\alpha} \left[F_n - c_o \left(\frac{3}{4} - c_{pa}\right) \frac{G_n n}{R}\right] \tag{23}$$

An uncertainty analysis of the aerodynamic-spring-constant equations is discussed in Appendix B.

The coefficients for the free-tip response equation have all been derived. An analysis defining the conditions for free-tip resonance is next described.

Free-Tip Pitching Resonance

An important objective of FTR research is avoiding resonant tip pitching oscillations. Given the derived approximate expressions for C_A and K_A, two important results can be derived for a free-tip subjected to periodic forcing.

The first result is an equation relating tip geometry and aerodynamics to the tip oscillation amplitude, expressed in terms of the magnification factor. The magnification factor (MF) is the ratio of a tip's actual oscillation amplitude to the tip displacement that would result from a statically applied moment equal in magnitude to the maximum periodic forcing.

The second result is the mathematical demonstration that tip resonance is dependent upon tip geometry and inertia but independent of tip speed, given the assumption that the aerodynamic forcing frequency is a linear function of Ω, which is justifiable because helicopter rotor aerodynamics and dynamics are often n/rev dependent.

Reference 11 defines MF to be

$$MF = \frac{\theta}{\theta_f} = \frac{1}{\sqrt{(1 - r_f^2)^2 + (2\zeta_d r_f)^2}} \tag{24}$$

where

$$r_f = \frac{\omega_f}{\omega} \quad \text{(forcing frequency ratio)}$$

$$\zeta_d = \frac{C_A}{2I\omega} \quad \text{(damping ratio)}$$

$$\omega = \sqrt{\frac{K_A}{I}} \quad \text{(tip natural frequency)}$$

The free-tip pitching-resonance analysis presented in this paper will be limited to pure sinusoidal forcing. The more complex case of general periodic forcing, like that of the whirl-test air jet or forward-flight rotor aerodynamics, will not be considered here. Additionally, it should be noted that tip-resonance analysis for a rotor in forward flight would require new aerodynamic spring and damping equations that include the effect of blade motion and unsteady inflow. However, such an extension could be made by representing the general periodic forcing by a Fourier series. The analysis will be further simplified by ignoring controller spring and damping contributions to the tip response.

The r_f and ζ_d terms in equation (24) need to be derived for an FTR free tip. The forcing-frequency ratio, r_f, will be derived first.

Let the forcing frequency be a linear function of Ω, or

$$\omega_f = b\Omega$$

In terms of tip speed

$$\omega_f = \frac{bV_T}{R}$$

(Note that if b is an integer, then the tip forcing frequency is n/rev.)

To complete the definition of r_f, it is necessary to derive an expression for the natural frequency of the free tip. To do so, the expressions for K_A and C_A must be substituted into the natural frequency definition. Note that the dependence of the aerodynamic spring on tip speed is parabolic while the damping coefficient is linear.

$$K_A = BV_T^2$$

where

$$B = \frac{1}{2}\rho\Delta R c_o^2\left(c_{pa} - \frac{1}{4}\right)\bullet C_{\ell_\alpha}\left[F_n - c_o\left(\frac{3}{4} - c_{pa}\right)\frac{G_n n}{R}\right] \tag{25a}$$

$$C_A = DV_T$$

and

$$D = \frac{1}{2}\rho\,\Delta R C_{\ell_\alpha}\left[c_o^3\left(\frac{1}{4} - c_{pa}\right)\left(\frac{3}{4} - c_{pa}\right)F_n + \frac{1}{n}c_o^2\left(\frac{1}{4} - c_{pa}\right)G_n R + \frac{1}{4}c_o^3\left(\frac{3}{4} - c_{pa}\right)\right] \tag{25b}$$

B and D are constants that are obtained from equations (19) and (23). Note that G_n and F_n are terms that are comprised of Bessel functions that are dependent only on k, the reduced frequency, and not on tip speed. The rotor rotational-speed terms are canceled out in the k expression (see equation (16c)).

Therefore, in terms of the above defined constants

$$\omega = \sqrt{\frac{K_A}{I}} = \sqrt{\frac{B}{I}}\,V_T$$

and so, from the previous work

$$r_f = \frac{\omega_f}{\omega} = \sqrt{\frac{I}{B}}\left(\frac{b}{R}\right) \tag{26}$$

Therefore, r_f is independent of tip speed.

An expression will now be derived for ζ_d, the damping ratio. Substituting the C_A and K_A functional expressions into the ζ_d definition results in the relation

$$\zeta_d = \frac{C_A}{2I\omega} = \frac{DV_T}{2I\sqrt{\frac{B}{I}}\,V_T} \qquad (27)$$

$$\zeta_d = \frac{D}{2\sqrt{IB}}$$

The damping ratio is also independent of tip speed.

The MF has been shown by equations (24)-(27) to be independent of rpm. Therefore, as long as the assumptions $\omega_f \approx b\Omega$ and $K \ll K_A$ hold true, then free-tip resonance (MF > 1 and $r_f \approx 1$) will not be initiated by rpm changes. Additionally, it should be noted that the solution of equation (19) cannot result in a negative estimate for C_A. Therefore, the damping analysis indicates that free-tip oscillations will be stable in hover.

COMPARISONS BETWEEN ANALYTICAL AND EXPERIMENTAL RESPONSE COEFFICIENTS

Application of the coefficient regression algorithms to the experimental data revealed that both the coulomb only, the combined coulomb and viscous damping analysis options of the least squares method, and the linear-decay averaging method resulted in erroneous coefficient values. The results obtained by these methods were physically unrealistic, i.e., application of either method would frequently result in one of the coefficients being negative. While free tip responses were obviously underdamped and not self-excited, these results were considered invalid and were therefore not included in this paper.

It was found necessary for almost all curve-fits to exclude a portion of each response curve so as to avoid test-chamber corner aerodynamic-interference effects. The azimuthal location of the air jet was approximately $\psi = 190°$. Therefore, the curve fitting was often limited to data having azimuths greater than $\psi = 240°$. To better demonstrate the validity of the curve fits, the resulting curves were extrapolated into the excluded azimuth range. How well these two sets of curves match is an indication of both the magnitude of the corner-interference effects and the quality of the curve-fit. A good curve-fit based on experimental response-curve data with minimal interference effects has a smooth transition between the two curve segments. Unfortunately, there are few FTR-tip, transient response data sets with the above quality. Regardless of the quality of the data, however, the least squares method demonstrated itself to be inadequate for even the viscous damping only case. As can be seen from figures 14(a)-(f), it has the tendency to radically overshoot even those portions of the free-tip response curves not significantly affected by corner effects. Therefore, the coefficient estimates of the logarithmic decay averaging method will be primarily used for the following discussion.

K contributes only about 5% of the K_E value. K_A is approximately equal to K_E. Because of difficulty in defining β and ζ, as applied to equation (12), the K_A analytical prediction is compared to the experimental K_E estimates.

There was considerable difference between the error values for each estimate of K_E and C_A. Therefore, in comparing the experimental coefficients with the predictions from equations (19) and (23) it was advantageous to express the experimental results in terms of a weighted average that took into account relative error estimates. Given the error parameter, R_{E_i}, as defined by equations (8) through (10), a weighting function, W_i, can be defined:

$$W_i = \frac{R_{E_{ib}}}{R_{E_i}} \tag{28}$$

where $R_{E_{ib}}$ is the best, i.e., the smallest, envelope-error estimate found in the average ensemble.

Therefore, with this defined function, weighted averaging was performed by the following operations:

$$K_{E_{av}} = \frac{\sum_{i=1}^{N} W_i K_{E_i}}{\sum_{i=1}^{N} W_i} \tag{29a}$$

where K_i are the spring estimate values. Similarly defined:

$$C_{A_{av}} = \frac{\sum_{i=1}^{N} W_i C_{A_i}}{\sum_{i=1}^{N} W_i} \tag{29b}$$

Having obtained coefficient averages by the above method, an improved comparison can now be made. Figures 15 and 16 are plots of predicted and experimental spring and damping constants as a function of rotor rpm. The data includes both weighted averages and uncorrected estimates.

The predicted K_A and C_A values were based on C_{ℓ_α} estimates derived from semispan wind tunnel data, thereby partially taking into account viscous and three-dimensional effects. Compressibility effects were not included. However, the experimental C_{ℓ_α} correction provides only approximate predictions of K_A and C_A for the free tip. The swept-tapered tip C_{ℓ_α} used in the C_A and K_A calculations was 3.67 rad^{-1}. The nth harmonic used in the predicted aerodynamic spring and damping coefficient calculations was $n = 6/rev$. This value was chosen because it

agreed with the experimental transient response frequency. The selection of n was not critical, as K_A and C_A were not sensitive to the harmonic order chosen.

Establishing the validity of the linear and parabolic trends of the C_A and K_A predictions (with respect to V_T) are impossible given the limited amount, and scatter, of the experimental data. The experimental aerodynamic damping coefficients do demonstrate some agreement with the predictions. Almost all data points fall within the uncertainty limits of the analytical predictions. These uncertainty limits are calculated by the analysis in Appendix C (for K_A limits see Appendix D) and the parameter accuracies in table 4. The experimental K_A values, though, significantly disagree with the spring predictions. However, a number of points do fall within, or on, the uncertainty limits of the predicted aerodynamic spring. It is apparent, therefore, that final verification of the free-tip response analysis requires an improved data base in terms of both quality and quantity.

Finally, figures 17(a)-(c) compares the transient response behavior of the free tip given the analytical- and experimental-weighted-average dynamic coefficients for rotor speeds of V_T = 161, 198, 213 m/sec. The experimental tip time histories were not used for the final response comparisons. The nonlinear distortions of the experimental time histories make them inappropriate for comparison with the analytical predictions. The curves shown in figures 17(a)-(c) were generated by using one form of the free-tip response equation's analytical solution

$$\theta = \theta_o \, e^{-\zeta_d \omega t} \cos(\omega_d t)$$

where θ_o is the tip's deflection after encountering the air jet.

SUMMARY

A model FTR whirl test was conducted in a small, rectangular test chamber. The 16-ft diam model FTR underwent collective and rpm sweeps, with and without air-jet excitation of the free tips. Both rotor balance loads and tip, pitch-angle time histories were acquired. Unlike a previous wind-tunnel test of the FTR, significant tip oscillations were observed as a consequence of air-jet excitation. The free-tip transient response, with digital filtering, was found to be an approximate single degree of freedom, constant coefficient, viscously underdamped oscillatory system. However, some nonlinear behavior was observed distorting the transient response. This distortion was probably due to test-chamber corner aerodynamic-interference effects.

The results of this test are summarized below:

1. The FTR free tips responded to the air jet with an approximately 6/rev natural frequency.

2. Sufficient tip-response data was acquired to estimate free-tip aerodynamic spring and damping coefficients. Digital filtering and selective curve fitting were necessary to calculate the coefficients. The transient response curves only roughly approximate the theoretical exponentially decayed sinusoid. This was possibly due to the poor quality of the aerodynamic environment of the test chamber.

3. Using Theodorsen unsteady, potential-flow analysis analytical expressions for the tip aerodynamic spring and damping were developed, K_A and C_A.

4. Comparisons were made between the experimental and analytical C_A and K_A estimates. The aerodynamic spring values showed large disagreements. The damping values demonstrated fair agreement.

5. An analytical expression was developed that related tip geometry and aerodynamics to tip oscillation amplitude, subject to a forcing function having a frequency that is dependent upon a first order polynomial of Ω. It was also analytically shown that in hover FTR tip pitching resonance is independent of tip speed.

6. Limited whirl-test rotor performance data was acquired for low C_T/σ. Baseline rigid-tip data was not acquired. However, rotor performance data for two controller control moments was obtained. No significant performance differences were noted for the two controller output settings.

7. Another free-tip whirl test should be conducted to provide a higher-quality data set. Only with such a data set will the analytical K_A and C_A models be completely verified.

APPENDIX A

DIFFERENTIAL EQUATION LEAST SQUARES REGRESSION METHOD

In order to estimate the spring and damping coefficients a curve fit of the experimental data could be performed using the tip-response differential equation. A least-squares error function was defined by

$$E = \sum_{i=1}^{N} \left[C_A \dot{\theta}_i + K_E \theta_i + \mathrm{sgn}(\dot{\theta}_i) T_f - M_{I_i} \right]^2 \tag{A1}$$

where

$$M_{I_i} = -I\ddot{\theta}_i$$

is the experimental tip inertial moment. The remaining error-function terms comprise the predicted inertial moment. The functional form of E is

$$E = E(C_A, K_E, T_f)$$

The error function is subject to the minimization constraint

$$\frac{\partial E}{\partial x_i} = 0 \quad (i = 1,2,3,\ldots)$$

where x_i represents the coefficients to be determined by regression, i.e., C_A, K_E, and T_f. The above constraint results in the following set of equations

$$\frac{\partial E}{\partial I} = 2 \sum_{i=1}^{N} F_i \ddot{\theta}_i = 0 \tag{A2a}$$

$$\frac{\partial E}{\partial C_A} = 2 \sum_{i=1}^{N} F_i \dot{\theta}_i = 0 \tag{A2b}$$

$$\frac{\partial E}{\partial K_E} = 2 \sum_{i=1}^{N} F_i \theta_i = 0 \tag{A2c}$$

$$\frac{\partial E}{\partial T_f} = 2 \sum_{i=1}^{N} F_i \mathrm{sgn}(\dot{\theta}_i) = 0 \tag{A2d}$$

where for simplicity F_i is defined to be

$$F_i = C_A\dot{\theta}_i + K_E\theta_i + \text{sgn}(\dot{\theta}_i)T_f - M_{i_i} \tag{A2e}$$

The previous set of equations were used to define matrix equations for given damping assumptions: viscous damping only, coulomb damping only, and combined coulomb viscous damping. These assumptions could be implemented by the selective exclusion of constraints and parameters. Experimental data sets were used to calculate the matrix elements which then were solved by a Gauss-Jordon routine. The solution matrix contained the free-tip dynamic coefficients.

The experimental tip acceleration ($\ddot{\theta}_i$) was approximated numerically from the experimental tip, pitch-angle time-history. Numerical derivatives are inaccurate when applied to scattered data, even when incorporating higher-order terms. Yet, it was hoped that the data scatter would be minimal and that the constraint summations comprising the matrix elements would have a smoothing effect that would compensate for the derivative inaccuracy.

An additional problem with this least squares method is that it is extremely sensitive to forced-tip response behavior, such as that induced by test-chamber corner effects, and thereby providing inaccurate results. To compensate for the test-chamber aerodynamic influence on the response curve, all data-reduction methods had the capacity for excluding the forced-tip portion of the transient response.

APPENDIX B

LINEAR DECAY AVERAGING METHOD

The parameters K_E and T_f are evaluated by this method, which assumes coulomb damping only.

If the tip oscillation damping was completely due to friction, the peak-to-peak amplitude decay would be linear according to the relationship

$$\theta_{i+1} = \theta_i - \frac{4T_f}{K_E}$$

where θ_i and θ_{i+1} are adjacent tip oscillation peak amplitudes for each cycle.

Another consequence of assuming pure coulomb damping is that the tip-response frequency is unaffected by the amount of damping. Therefore,

$$\omega = \omega_d = \frac{2\pi}{\tau}$$

and the tip response frequency would be the natural frequency.

On a local basis, then, the parameters T_f and K_E can be estimated by the following equations.

$$\omega_i = \frac{2\pi}{\tau_i} \tag{B1}$$

$$K_{E_i} = I\omega_i^2 \tag{B2}$$

$$T_f = \frac{1}{4}(\theta_i - \theta_{i+1})K_{E_i} \tag{B3}$$

Finally, averaging is used to calculate a representative set of tip response coefficients.

More extensive discussion of coulomb-damped transient response can be found in reference 11.

APPENDIX C

AERODYNAMIC-DAMPING-COEFFICIENT UNCERTAINTY ANALYSIS

The aerodynamic damping coefficient was found to be

$$C_{A_n} = \frac{1}{2}\rho\,\Delta R C_{\ell_\alpha}\left[c_o^3\left(\frac{1}{4} - c_{pa}\right)\left(\frac{3}{4} - c_{pa}\right)F_n V_T + \frac{1}{n}\,c_o^2\left(\frac{1}{4} - c_{pa}\right)G_n R V_T + \frac{1}{4}\,c_o^3\left(\frac{3}{4} - c_{pa}\right)V_T\right]$$

C_{A_n} has the functional form

$$C_{A_n} = C_{A_n}(\rho, \Delta R, C_{\ell_\alpha}, V_T, c_o, c_{pa}, R, F_n, G_n)$$

By letting

$$C_1 = \left[c_o^3\left(\frac{1}{4} - c_{pa}\right)\left(\frac{3}{4} - c_{pa}\right)F_n V_T + \frac{1}{n}\,c_o^2\left(\frac{1}{4} - c_{pa}\right)G_n R V_T + \frac{1}{4}\,c_o^3\left(\frac{3}{4} - c_{pa}\right)V_T\right]$$

$$C_2 = \frac{1}{2}\rho\,\Delta R C_{\ell_\alpha} V_T$$

The following partial derivatives can be defined

$$\frac{\partial C_A}{\partial \rho} = \frac{1}{2}\,\Delta R C_{\ell_\alpha} V_T C_1 \tag{C1a}$$

$$\frac{\partial C_A}{\partial \Delta R} = \frac{1}{2}\,\rho C_{\ell_\alpha} V_T C_1 \tag{C1b}$$

$$\frac{\partial C_A}{\partial C_{\ell_\alpha}} = \frac{1}{2}\,\rho\,\Delta R V_T C_1 \tag{C1c}$$

$$\frac{\partial C_A}{\partial V_T} = \frac{1}{2}\,\rho\,\Delta R C_{\ell_\alpha} C_1 \tag{C1d}$$

$$\frac{\partial C_A}{\partial C_o} = C_2\left[3c_o^2\left(\frac{1}{4} - c_{pa}\right)\left(\frac{3}{4} - c_{pa}\right)F_n + \frac{2}{n}\,c_o\left(\frac{1}{4} - c_{pa}\right)G_n R + \frac{3}{4}\,c_o^2\left(\frac{3}{4} - c_{pa}\right)\right] \tag{C1e}$$

$$\frac{\partial C_A}{\partial c_{pa}} = C_2\left[c_o^3 F_n(2c_{pa} - 1) - \frac{1}{n}\,G_n R c_o^2 - \frac{1}{4}\,c_o^3\right] \tag{C1f}$$

$$\frac{\partial C_A}{\partial R} = C_2\left(\frac{1}{n}\right)c_o^2\left(\frac{1}{4} - c_{pa}\right)G_n \tag{C1g}$$

$$\frac{\partial C_A}{\partial F_n} = C_2\left(\frac{3}{4} - c_{pa}\right)c_o^3\left(\frac{1}{4} - c_{pa}\right) \tag{C1h}$$

$$\frac{\partial C_A}{\partial G_n} = C_2\left(\frac{1}{n}\right)c_o^2\left(\frac{1}{4} - c_{pa}\right)R \tag{C1i}$$

The uncertainty in F_n and G_n is governed by the uncertainty in k, the reduced frequency. Noting

$$k = \frac{c_o n\Omega}{2V_T} = \frac{c_o n}{2R}$$

where functionally

$$k = k(c_o, R)$$

Its partial derivatives are therefore

$$\frac{\partial k}{\partial c_o} = \frac{n}{2R} \tag{C2a}$$

$$\frac{\partial k}{\partial R} = -\frac{c_o n}{2R^2} \tag{C2b}$$

A computer algorithm was developed to perform the C_A uncertainty calculations. The uncertainty analysis is based upon a method presented in reference 12. This method requires the definition of the previous derivatives to define ω_{C_A}, the uncertainty of the predicted C_A. One simplifying approximation used in the C_A uncertainty calculation is the uncertainty estimate for $Y_1(k)$, $Y_o(k)$: only the accuracy of the reduced frequency is considered. The accuracy of the Bessel functions $J_o(k)$ and $J_1(k)$ influencing the accuracy of $Y_o(k)$ and $Y_1(k)$ is not incorporated into the uncertainty analysis.

The uncertainty of F_n and G_n can now be estimated once the Bessel function uncertainties have been estimated from the k accuracy estimate.

$$G_n = \frac{J_1(Y_1 - J_o) - Y_1(J_1 + Y_o)}{(Y_1 - J_o)^2 + (J_1 + Y_o)^2}$$

where

$$G_n = G_n\ (J_o, Y_o, J_1, Y_1)$$

Letting

$$G1 = J_1(Y_1 - J_o) - Y_1(J_1 + Y_o)$$

$$G2 = (Y_1 - J_o)^2 + (J_1 + Y_o)^2$$

The G_n derivatives are

$$\frac{\partial G_n}{\partial J_o} = \frac{-J_1}{G2} + \frac{2G1(Y_1 - J_o)}{G2^2} \qquad \text{(C3a)}$$

$$\frac{\partial G_n}{\partial Y_o} = \frac{-Y_1}{G2} - \frac{2G1(J_1 + Y_o)}{G2^2} \qquad \text{(C3b)}$$

$$\frac{\partial G_n}{\partial J_1} = \frac{-J_o}{G2} - \frac{2G1(J_1 + Y_o)}{G2^2} \qquad \text{(C3c)}$$

$$\frac{\partial G_n}{\partial Y_1} = \frac{-Y_o}{G2} - \frac{2G1(Y_1 - J_o)}{C2^2} \qquad \text{(C3d)}$$

Similarly for F_n

$$F_n = \frac{J_1(J_1 + Y_o) + Y_1(Y_1 + J_o)}{(Y_1 - J_o)^2 + (J_1 + Y_o)^2}$$

where

$$F_n = F_n(J_o, Y_o, J_1, Y_1)$$

Letting

$$F1 = J_1(J_1 + Y_o) + Y_1(Y_1 - J_o)$$

$$F2 = (Y_1 - J_o)^2 + (J_1 + Y_o)^2$$

The F_n partial derivatives are

$$\frac{\partial F_n}{\partial J_o} = \frac{-Y_1}{F2} + \frac{2F1(Y_1 - J_o)}{F2^2} \tag{C4a}$$

$$\frac{\partial F_n}{\partial Y_o} = \frac{J_1}{F2} - \frac{2F1(J_1 + Y_o)}{F2^2} \tag{C4b}$$

$$\frac{\partial F_n}{\partial J_1} = \frac{(2J_1 + Y_o)}{F2} - \frac{2F1(J_1 + Y_o)}{F2^2} \tag{C4c}$$

$$\frac{\partial F_n}{\partial Y_1} = \frac{(2Y_1 - J_o)}{F2} - \frac{2F1(Y_1 - J_o)}{F2^2} \tag{C4d}$$

The final step in defining the uncertainty of the predicted C_A results, ω_{C_A}, can be accomplished by the following general expression (ref. 12).

$$\omega_C = \left[\sum_{i=1}^{N} \left(\frac{\partial C}{\partial x_i}\,\omega_{x_i}\right)^2\right]^{1/2}$$

where x_i represents all the independent parameters, ω_{X_i} is the estimated accuracy of each independent parameter, and ω_C is the uncertainty of the dependent (calculated) parameter, C.

Therefore, for C_A the previous expression becomes

$$\omega_{C_A} = \left[\left(\frac{\partial C_A}{\partial \rho}\,\omega_\rho\right)^2 + \left(\frac{\partial C_A}{\partial \Delta R}\,\omega_{\Delta R}\right)^2 + \ldots\right]^{1/2} \tag{C5}$$

The predicted aerodynamic damping uncertainty can be calculated by first using the parameter values and accuracies in table 4 to calculate the partial derivatives, equations (C1)-(C4). Equation (C5) is then used to calculate ω_{C_A}. For the swept and tapered free tip used in this test, ω_{C_A} was typically 41% of the predicted C_A values.

APPENDIX D

AERODYNAMIC SPRING UNCERTAINTY ANALYSIS

The aerodynamic spring equation was found to be

$$K_{A_n} = \frac{1}{2} \rho \, \Delta R V_T^2 c_o^2 \left(\frac{1}{4} - c_{pa}\right) \cdot C_{\ell_\alpha} \left[F_n - c_o \left(\frac{3}{4} - c_{pa}\right) \frac{G_n n}{R}\right]$$

Therefore, in functional form

$$K_{A_n} = K_{A_n}\left(\rho, \Delta R, V_T, c_o, c_{pa}, C_{\ell_\alpha}, F_n, G_n, R\right)$$

By letting

$$K_1 = c_o^2 \left(c_{pa} - \frac{1}{4}\right) C_{\ell_\alpha} \left[F_n - c_o \left(\frac{3}{4} - c_{pa}\right) \frac{G_n n}{R}\right]$$

$$K_2 = \frac{1}{2} \rho \, \Delta R V_T^2$$

The partial derivatives are then

$$\frac{\partial K_A}{\partial \rho} = \frac{1}{2} \Delta R V_T^2 K_1 \tag{D1a}$$

$$\frac{\partial K_A}{\partial \Delta R} = \frac{1}{2} \rho V_T^2 K_1 \tag{D1b}$$

$$\frac{\partial K_A}{\partial V_T} = \rho \, \Delta R V_T K_1 \tag{D1c}$$

$$\frac{\partial K_A}{\partial c_o} = K_2 C_{\ell_\alpha} \left[2c_o \left(c_{pa} - \frac{1}{4}\right) F_n - 3c_o^2 \left(c_{pa} - \frac{1}{4}\right)\left(\frac{3}{4} - c_{pa}\right) \frac{G_n n}{R}\right] \tag{D1d}$$

$$\frac{\partial K_A}{\partial c_{pa}} = K_2 C_{\ell_\alpha} \left[c_o^2 F_n + c_o^3 \left(\frac{G_n n}{R}\right) (2c_{pa} - 1)\right] \tag{D1e}$$

$$\frac{\partial K_A}{\partial C_{\ell_\alpha}} = K_2 c_o^2 \left(c_{pa} - \frac{1}{4}\right) \left[F_n - c_o \left(\frac{3}{4} - c_{pa}\right) \frac{G_n n}{R}\right] \tag{D1f}$$

$$\frac{\partial K_A}{\partial R} = K_2 c_o^3 \left(c_{pa} - \frac{1}{4}\right)\left(\frac{3}{4} - c_{pa}\right) C_{\ell_\alpha} \left(\frac{G_n n}{R^2}\right) \tag{D1g}$$

$$\frac{\partial K_A}{\partial F_n} = K_2 c_o^2 \left(c_{pa} - \frac{1}{4}\right) C_{\ell_\alpha} \tag{D1h}$$

$$\frac{\partial K_A}{\partial G_n} = K_2 c_o^3 \left(c_{pa} - \frac{1}{4}\right) C_{\ell_\alpha} \left(\frac{3}{4} - c_{pa}\right)\left(\frac{n}{R}\right) \tag{D1i}$$

Finally, to estimate $\partial K_A/\partial F_n$ and $\partial K_A/\partial G_n$ the contribution of k, the reduced frequency, must be incorporated into the uncertainty analysis (refer to Appendix C).

The uncertainty analysis method of reference 12 is used to determine the uncertainty of the predicted K_A results, i.e., ω_{K_A}. Using table 4 parameter values and accuracies the K_A partial derivatives can be calculated and substituted into an uncertainty estimate equation similar to equation C5. Typical ω_{K_A} values are 39% of the predicted K_A values of the free tips that are whirl-tested.

REFERENCES

1. Stroub, Robert H.: A Constant Lift Rotor for a Heavier-than-Air Craft. U.S. Patent 4,137,010: January 30, 1979.

2. Stroub, Robert H.: Performance Improvements with the Free Tip Rotor. AHS National Specialists' Meeting, Rotor System Design, Oct. 1980.

3. Stroub, Robert H.: An Analytical Investigation of the Free-Tip Rotor for Helicopters. NASA TM-81345, 1982.

4. McVeigh, M. A.; Rosenstein, H.; Bartie, K.; and McHugh, F. J.: Investigation of a Rotor System Incorporating a Constant-Lift Tip. NASA CR-166361, 1981.

5. Stroub, Robert H.: An Experimental Investigation of a Free-Tip Rotor Configuration in a Forward Flight Wind-Tunnel Test. NASA TM-84409, 1983.

6. Chopra, I.: Dynamic Analysis of a Free-Tip Rotor. AIAA Paper 81-0618-CP, 1981.

7. Kumagai, Hiroyuki: A Feasibility Study of Free-Tip Rotor Application as a Passive Cyclic Control Device. NASA CR-166608, 1984.

8. Bielawa, Richard L.: Analytic Investigation of Helicopter Rotor Blade Appended Aeroelastic Devices. NASA CR-166525, 1984.

9. Young, Larry A.: The Evaluation of a Number of Prototypes for the Free-Tip Rotor Constant Moment Controller. NASA TM-86664, 1985.

10. Yates, Leslie; and Kumagai, Hiroyuki: Application of Two-Dimensional Unsteady Aerodynamics to a Free-Tip Rotor Response Analysis. NASA CR-177348, 1985.

11. Vierck, Robert K.: Vibration Analysis. Second ed., Harper & Row, 1979.

12. Homan, J. P.; and Gajda, W. J., Jr.: Experimental Methods for Engineers. Third ed., McGraw-Hill, 1978.

TABLE 1.- ROTOR AND FREE-TIP GEOMETRY

Model rotor (dimensions include free tips)	
Radius	2.56 m
Number of blades	4
Chord	0.171 m (constant to 0.9R)
Solidity	0.085
Twist (center of rotation to tip)	-9.45° (for $\Delta\theta = 0$)
Airfoils	V23010-1.58 (constant)
Cutout	0.1825R
Flap-hinge offset	0.031R
Weight moment about flap hinge	46.8 N-m
Inertia about flap hinge	6.17 kg - m^2
Free-tip geometry (10% tip)	
Extends over outboard 10% of rotor radius	
0.30 taper ratio over outboard 5% of blade radius	
35° of 1/4 chord sweep over outboard 5% of blade radius	
V23010 - 1.58 with 0° tab angle	
Tip twist, -0.94°	
Pitch axis, 13% of chord	
Center of gravity located at 14% chord	

TABLE 2.- HARMONIC COEFFICIENTS FOR TEST DATA POINTS

Whirl-test rotor rpm	796		740		600	
Test data point	1	2	3	4	5	6
Coefficient						
A_1	0.212	0.334	0.485	0.212	0.371	0.408
A_2	-.019	-.051	-.087	-.018	-.063	-.121
A_3	.062	.097	.079	.054	.180	.181
A_4	-.137	-.176	-.188	-.085	-.127	-.284
A_5	.069	.175	.193	.053	.141	.291
A_6	-.015	-.077	-.112	-.022	-.112	-.247
A_7	.025	.066	.096	.015	.069	.174
A_8	.000	-.027	-.099	-.030	-.055	-.100
A_9	-.016	-.009	-.002	.016	.033	.047
A_{10}	-.008	.000	-.009	-.002	-.011	.014
B_1	.057	.161	.268	.061	.086	.245
B_2	-.067	-.095	-.056	.001	-.064	-.184
B_3	.055	.045	.113	.047	.061	.111
B_4	-.029	-.065	-.099	-.014	-.057	-.142
B_5	-.056	-.018	.044	-.009	.005	.063
B_6	.048	.069	.064	.018	.076	.125
B_7	-.033	-.070	-.051	-.015	-.046	-.137
B_8	.039	.093	.064	.018	.059	.132
B_9	-.023	-.023	-.117	-.007	-.050	-.133
B_{10}	.018	.042	.053	.016	.071	.158

The averaged free-tip response can be represented by a Fourier series

$$\theta = \sum_{n=1}^{10} [A_n \sin(nt) + B_n \cos(nt)]$$

where $A_1, \ldots, A_{10}$ and $B_1, \ldots, B_{10}$ can be obtained from the above table for six test points and three different rotor rpm's.

TABLE 3.- DATA-REDUCTION ALGORITHMS MATRIX

Data-reduction method	Calculates free-tip spring	Calculates free-tip viscous-damping	Calculates free-tip coloumb-damping
Differential-equation least-squares fit (complete coefficient set)	Yes	Yes	Yes
Differential-equation least-squares fit (partial coefficient set)	Yes	Yes	No
Logarithmic-decrement averaging	Yes	Yes	No
Linear-decay averaging	Yes	No	Yes

TABLE 4.- FREE-TIP AERODYNAMIC SPRING AND DAMPING PARAMETERS AND ACCURACY

ρ	1.227×10^{-5} kg/m^3	$\pm1.227\times10^{-6}$
ΔR	0.2097 m	±0.0210
$C_{\ell\alpha}$	0.064 deg^{-1}	±0.0064
C_o	0.1710 m	±0.0171
C_{pa}	0.13% chord	±0.013
V_t	188.4578 mps	±2.5603
R	2.4384 m	±0.0610

Figure 1.- FTR.

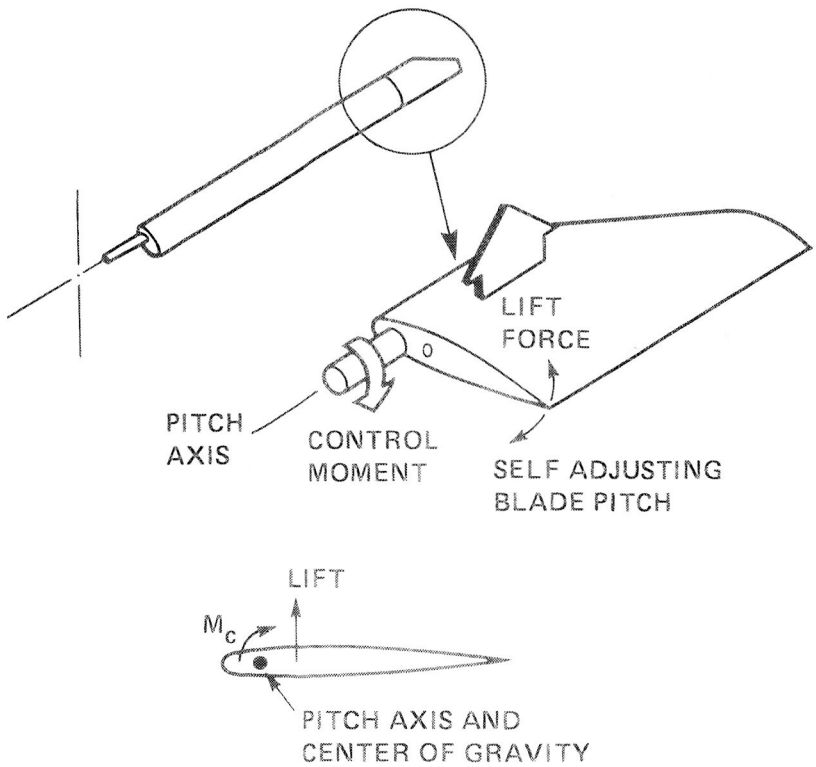

Figure 2.- FTR concept.

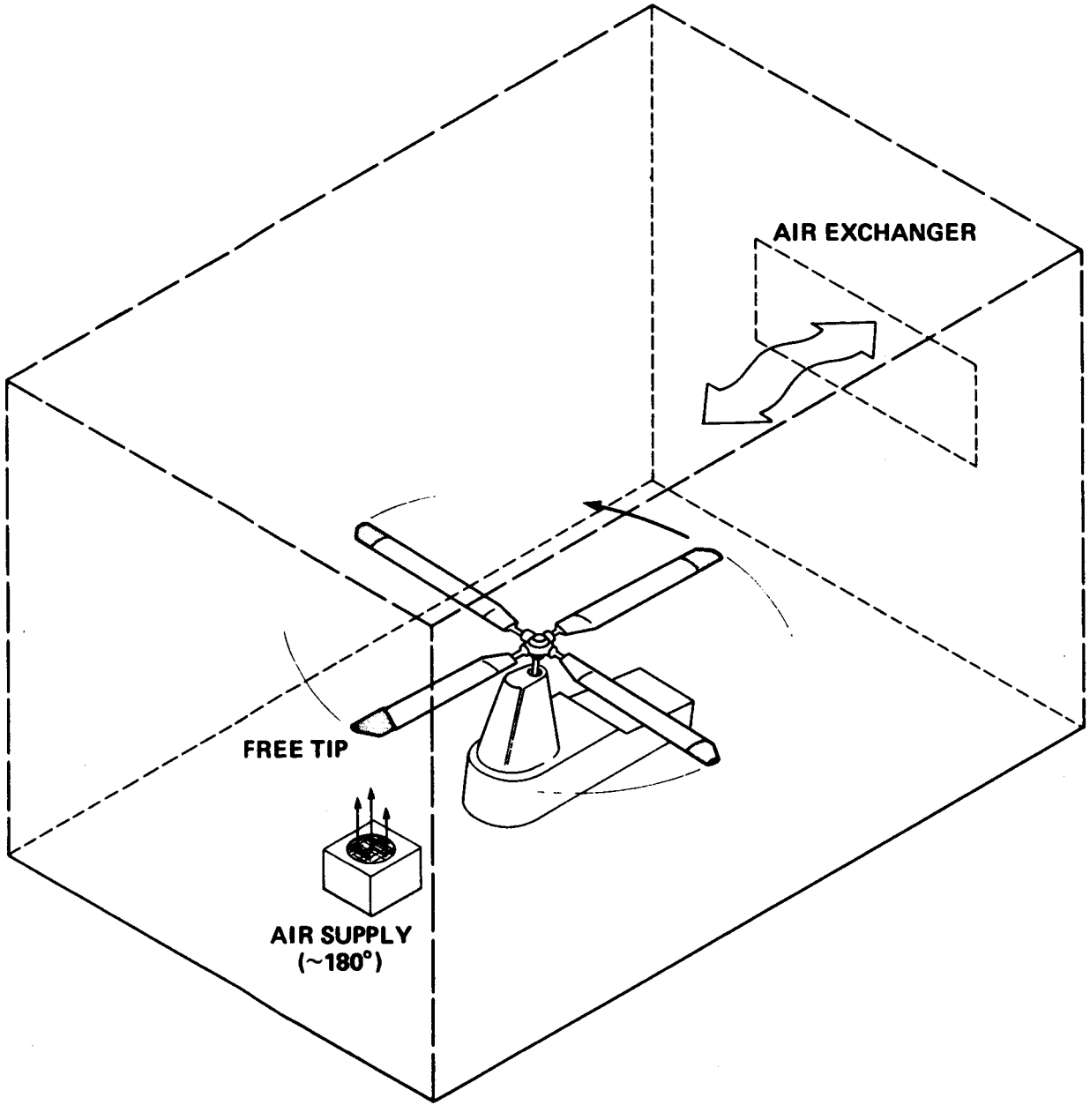

Figure 3.- FTR installed in test chamber.

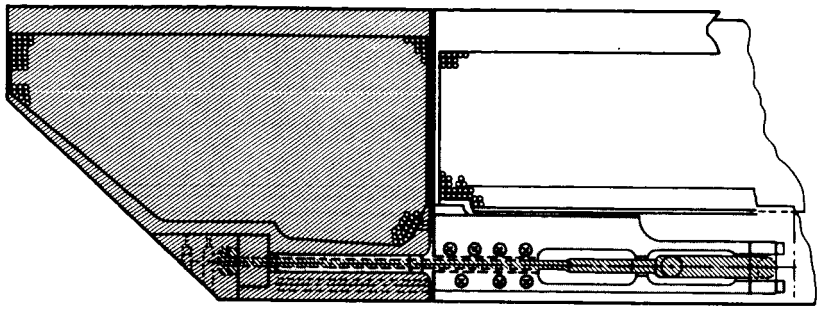

Figure 4.- Controller and rotor tip assembly.

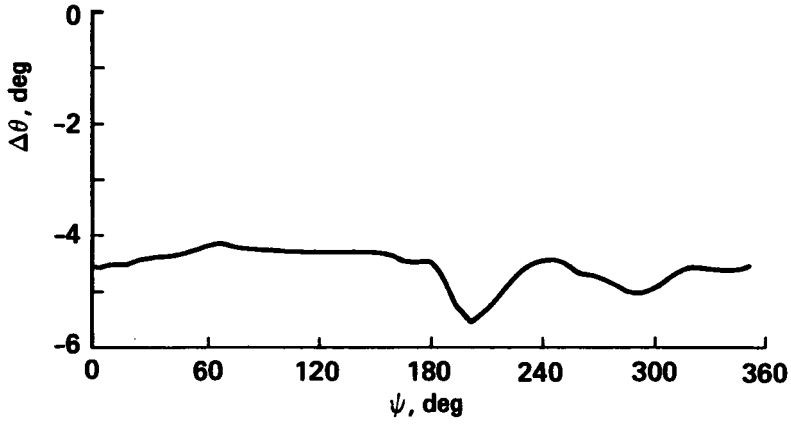

Figure 5.- Free-tip jet response time history.

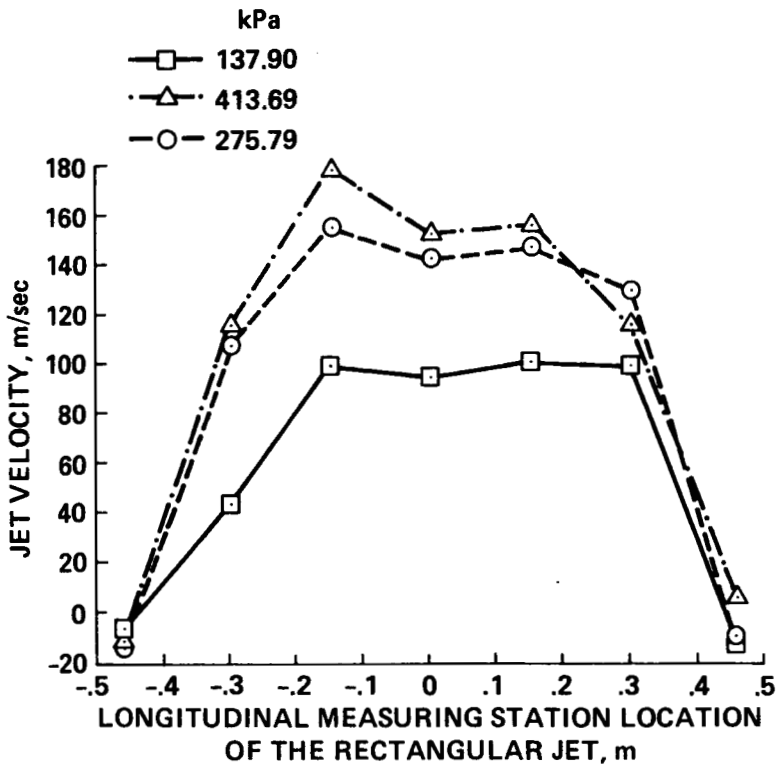

(a) Jet-velocity profile in the rotor tip path direction (vertical distance from the jet = 0.46 m).

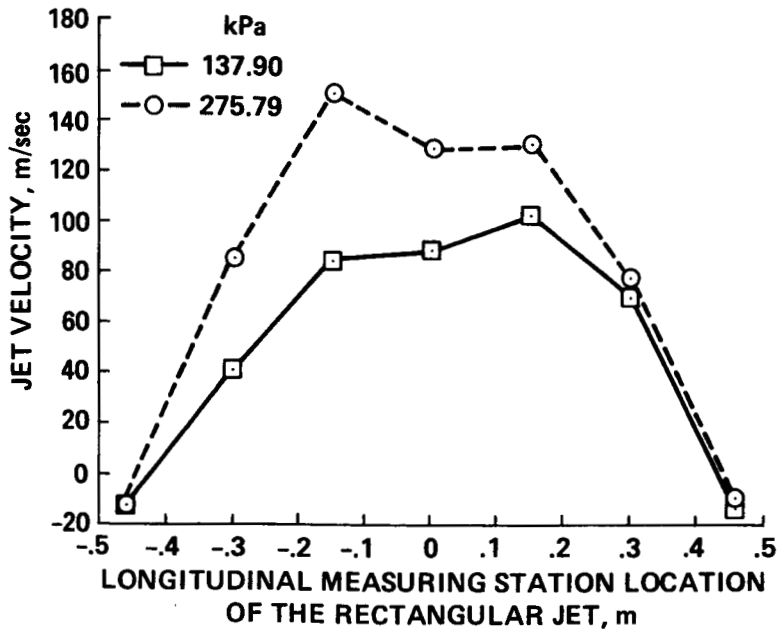

(b) Jet-velocity profile in the rotor tip path direction (vertical distance from the jet = 0.76 m).

Figure 6.- Measured air-jet velocity distributions.

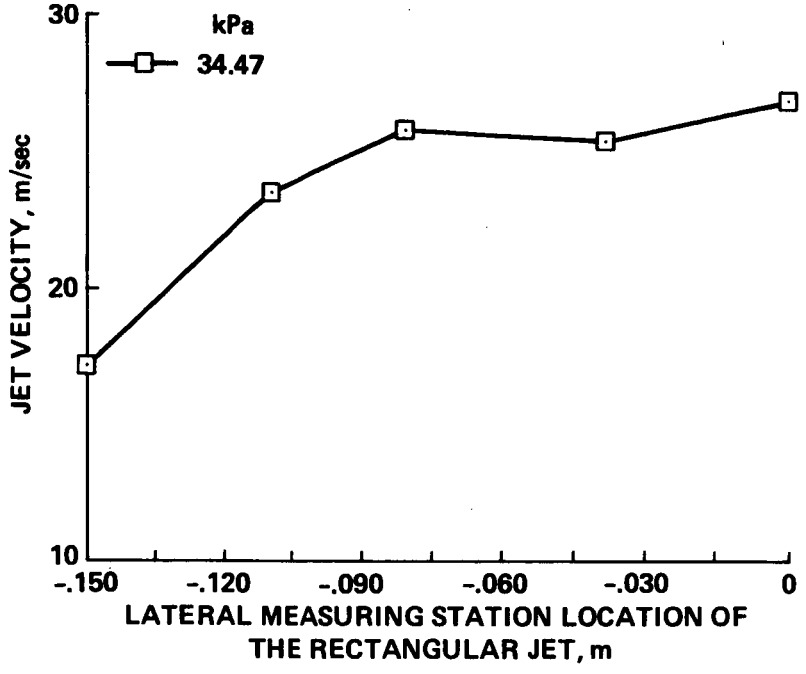

(c) Jet-velocity profile in the rotor spanwise direction (vertical distance from the jet = 1.83 m).

Figure 6.- Concluded.

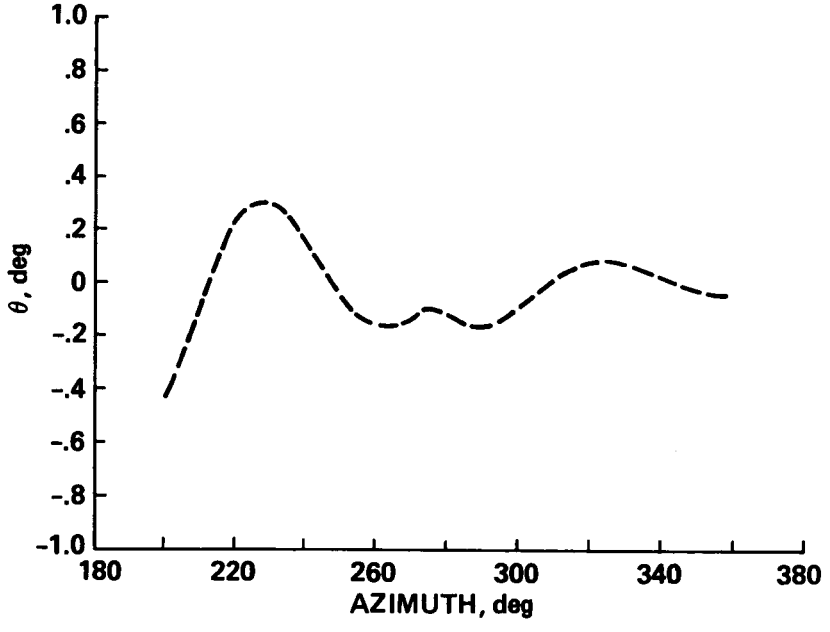

Figure 7.- Experimental free-tip jet-response time history, digitally filtered.

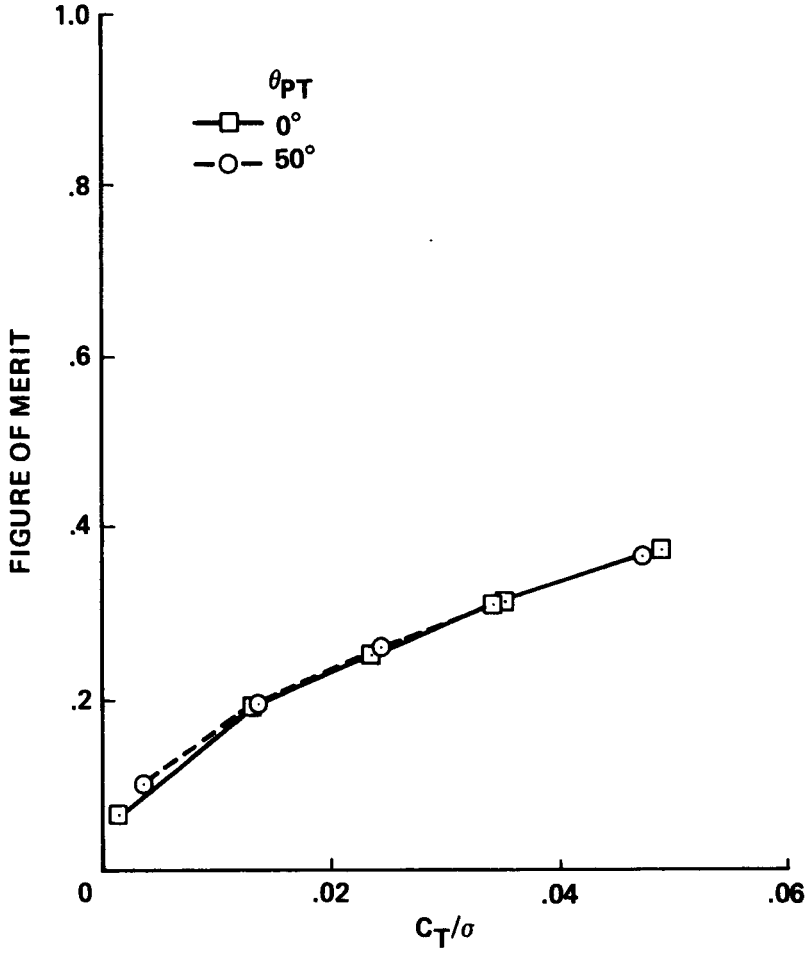

Figure 8.- FTR figure-of-merit curve for different controller pretwist angles.

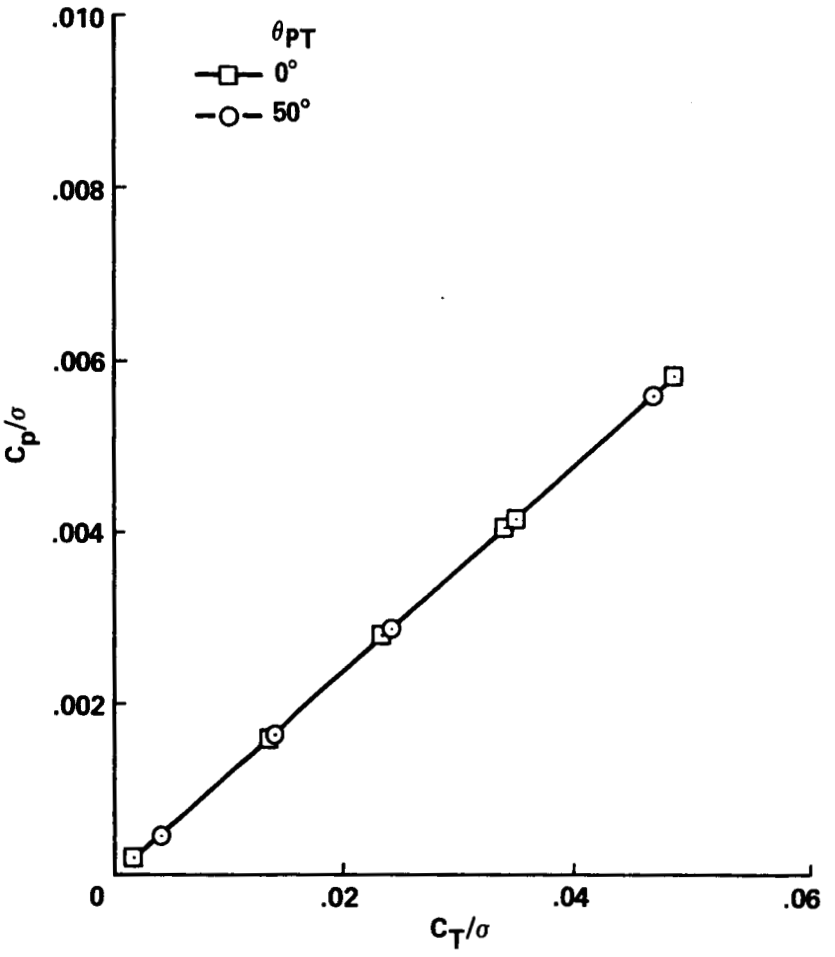

Figure 9.- FTR power vs. thrust curve for different controller pretwist angles.

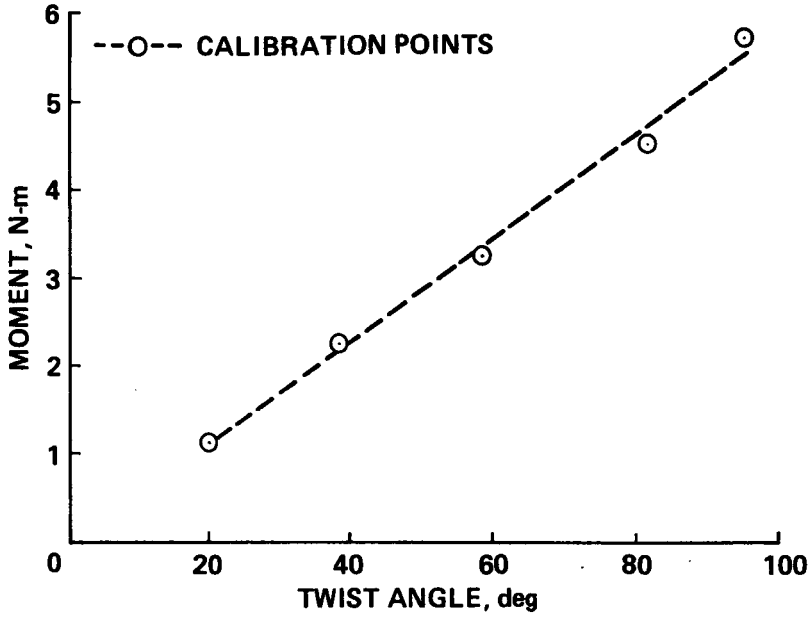

(a) TSC moment vs. twist characteristics.

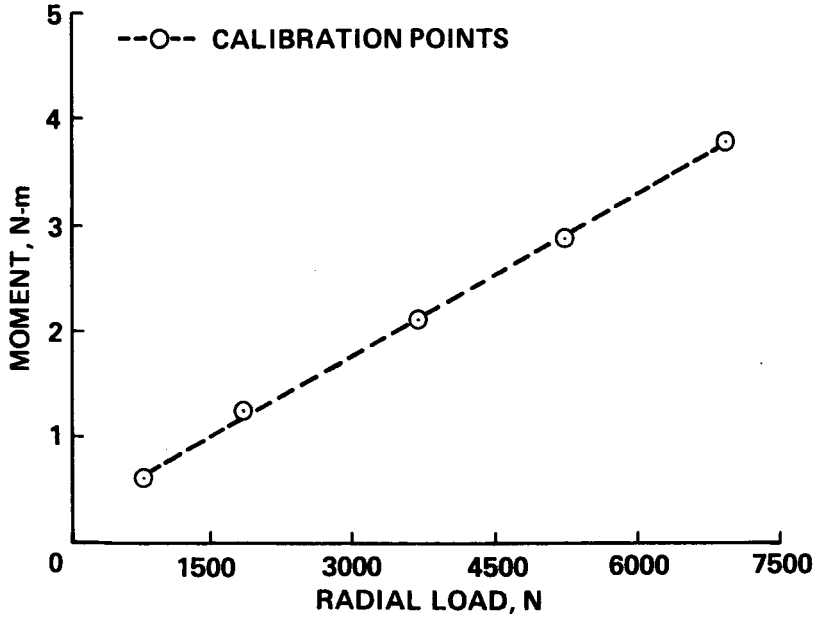

(b) TSC moment vs. tensile load characteristics.

Figure 10.- Free-tip torsion-strap controller pull test results.

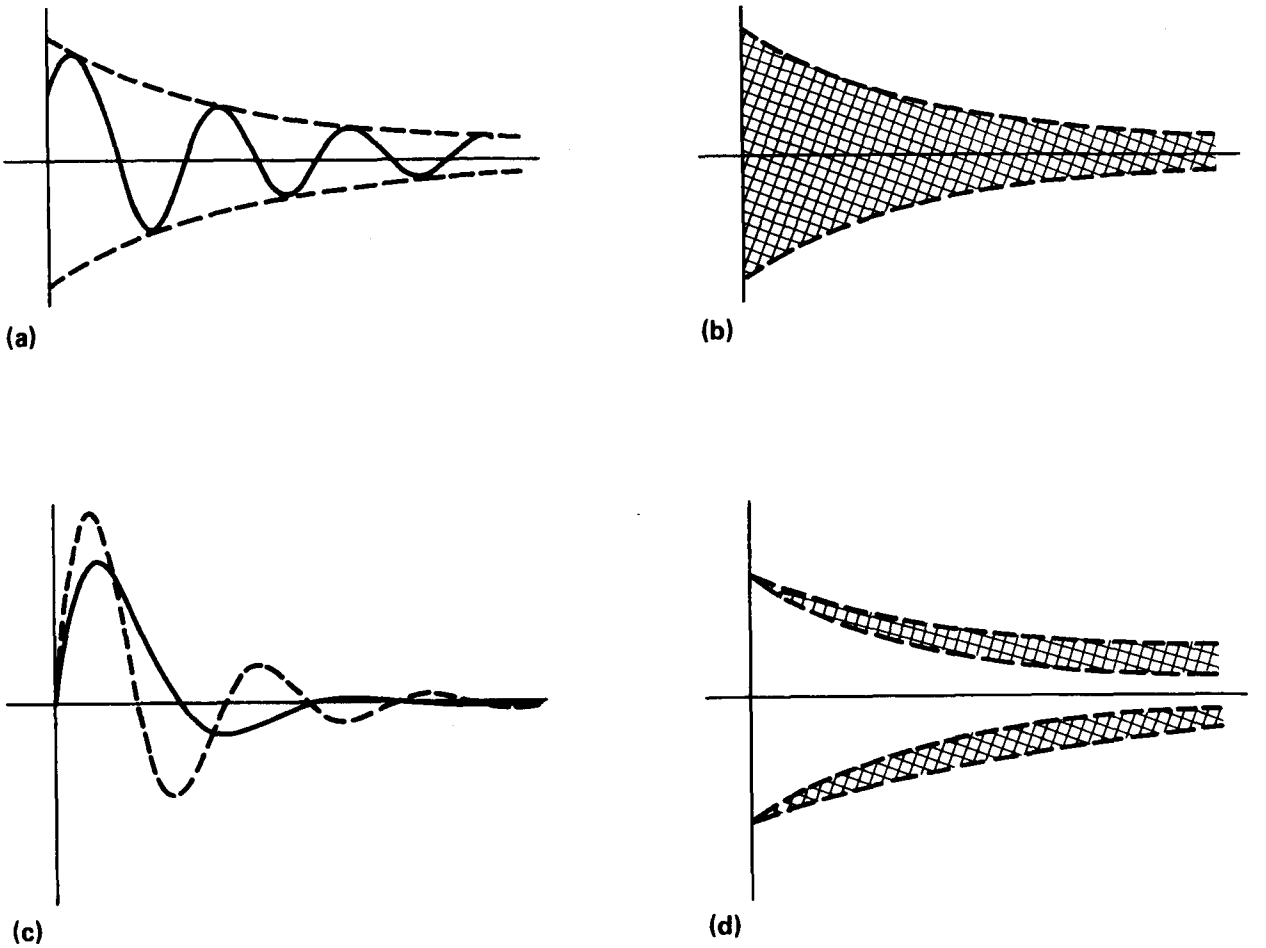

Figure 11.- The envelope-area error estimate. (a) Transient response with envelope outlined. (b) The envelope area. (c) Curve-fitted response and experimental data. (d) The resulting envelope area comparison.

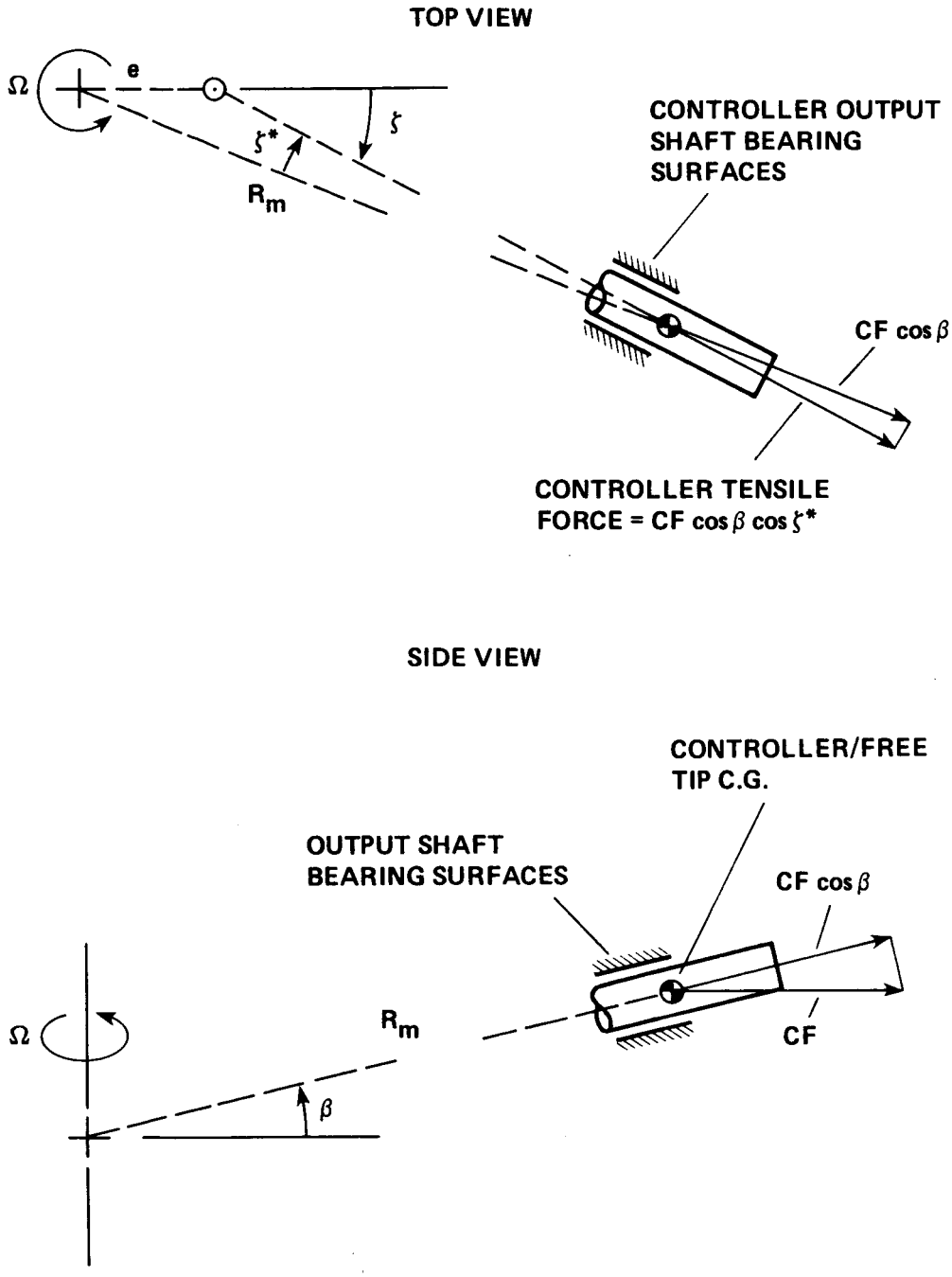

Figure 12.- A freebody diagram of the force components contributing to the controller straps' tensile load.

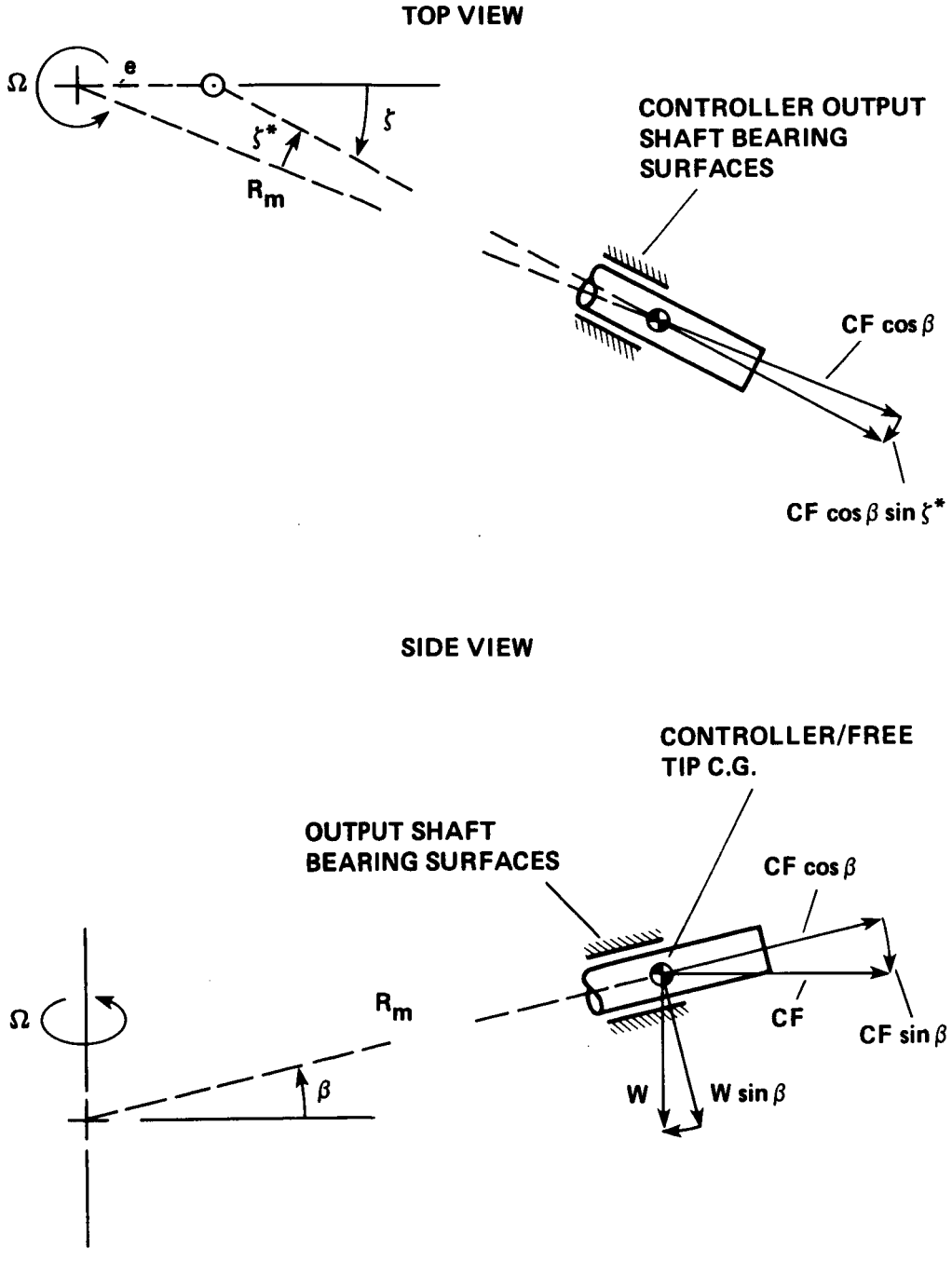

Figure 13.- A freebody diagram of the force components contributing to the controller bearings' contact force.

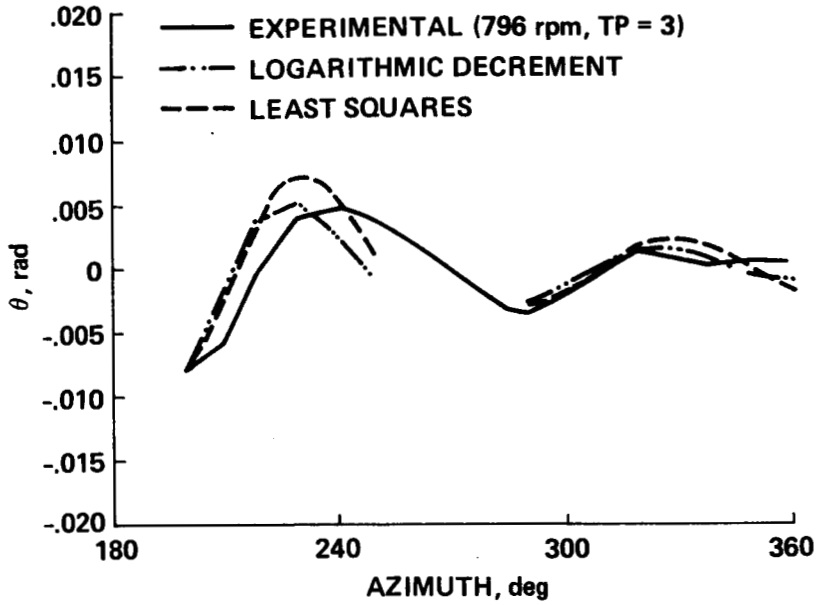

(a) Test point 1 averaged transient response, 796 rpm.

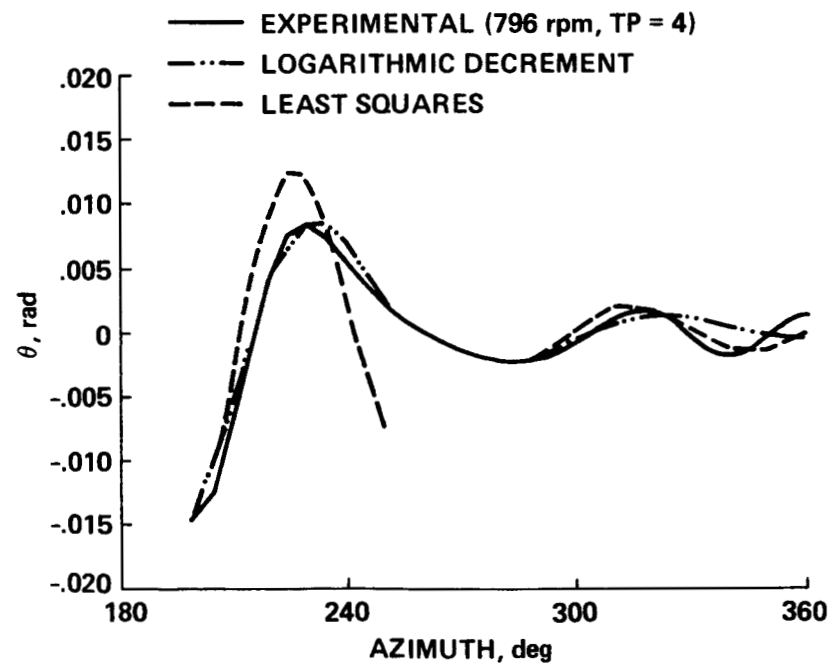

(b) Test point 2 averaged transient response, 796 rpm.

Figure 14.- The filtered free-tip transient responses used for the spring and damping estimates. (Curve-fit results also shown.)

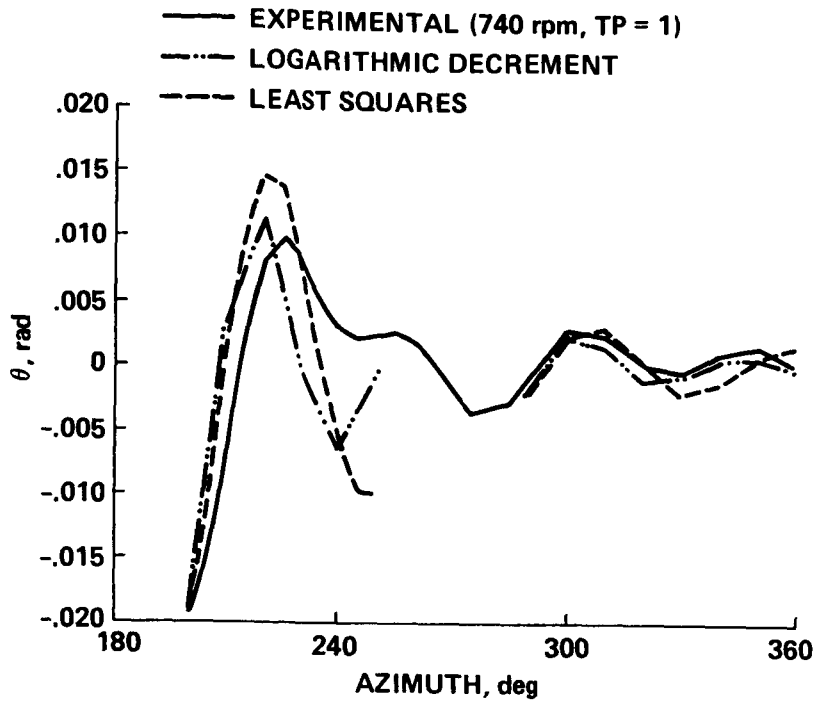

(c) Test point 3 averaged transient response, 740 rpm.

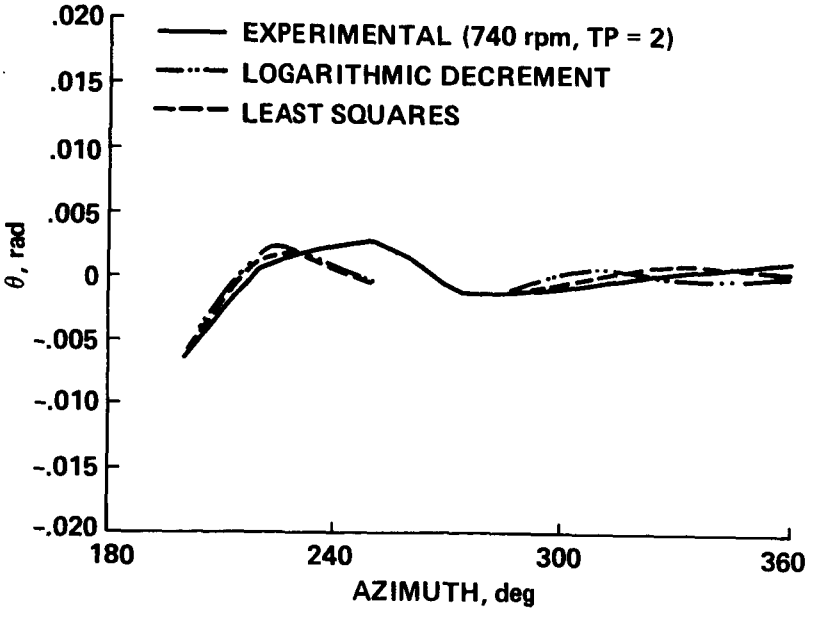

(d) Test point 4 averaged transient response, 740 rpm.

Figure 14.- Continued.

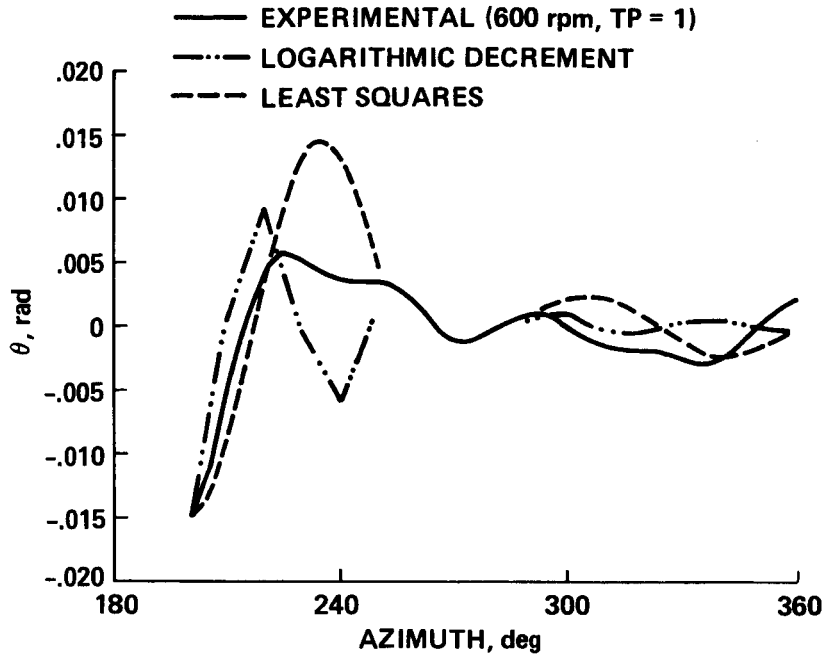

(e) Test point 5 averaged transient response, 600 rpm.

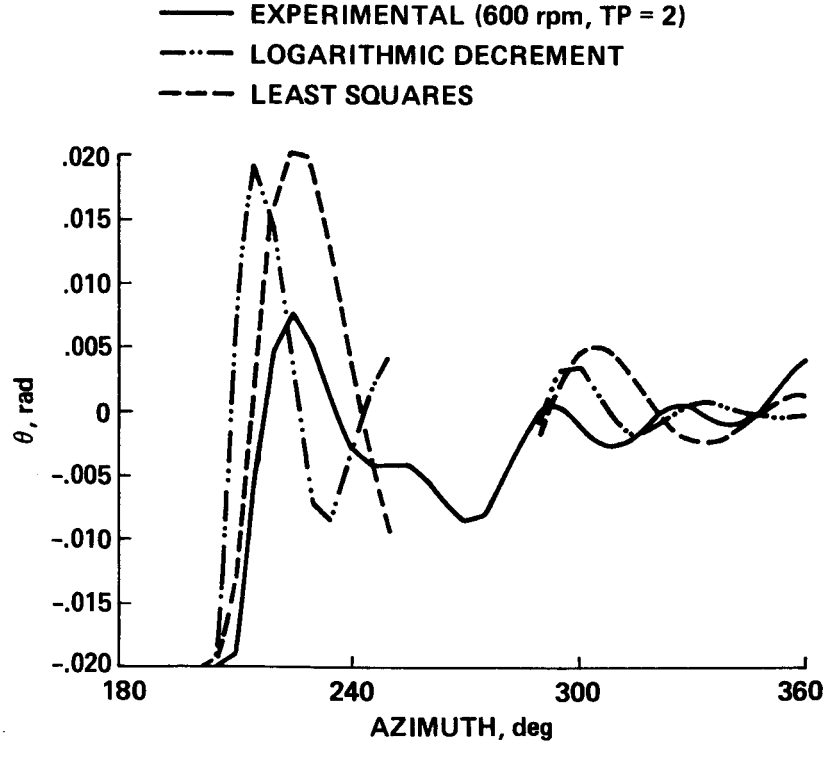

(f) Test point 6 averaged transient response, 600 rpm.

Figure 14.- Concluded.

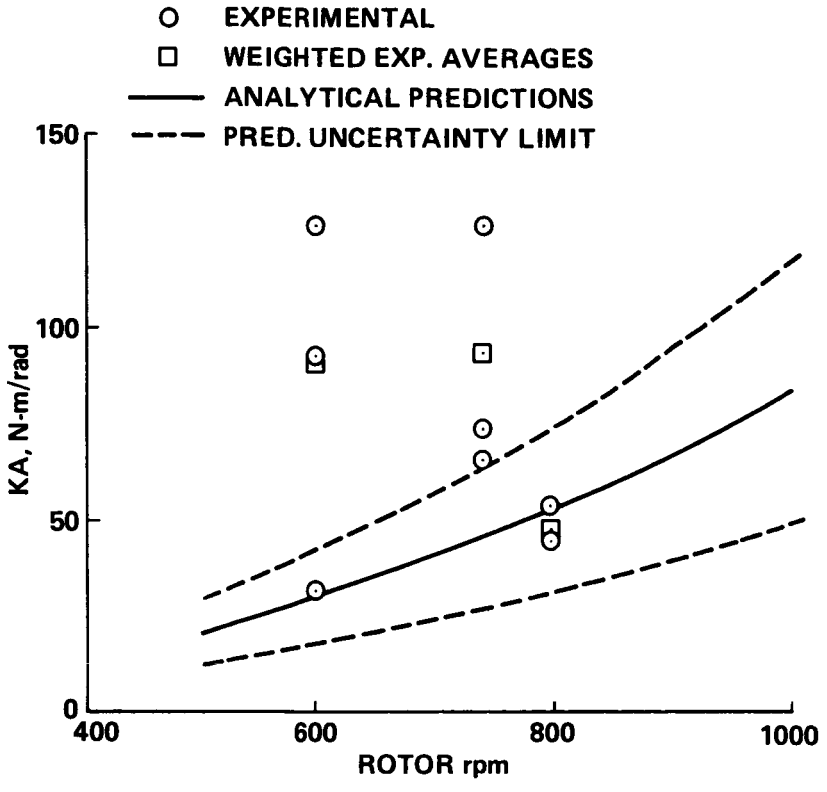

Figure 15.- Free-tip aerodynamic-spring analytical and experimental comparison.

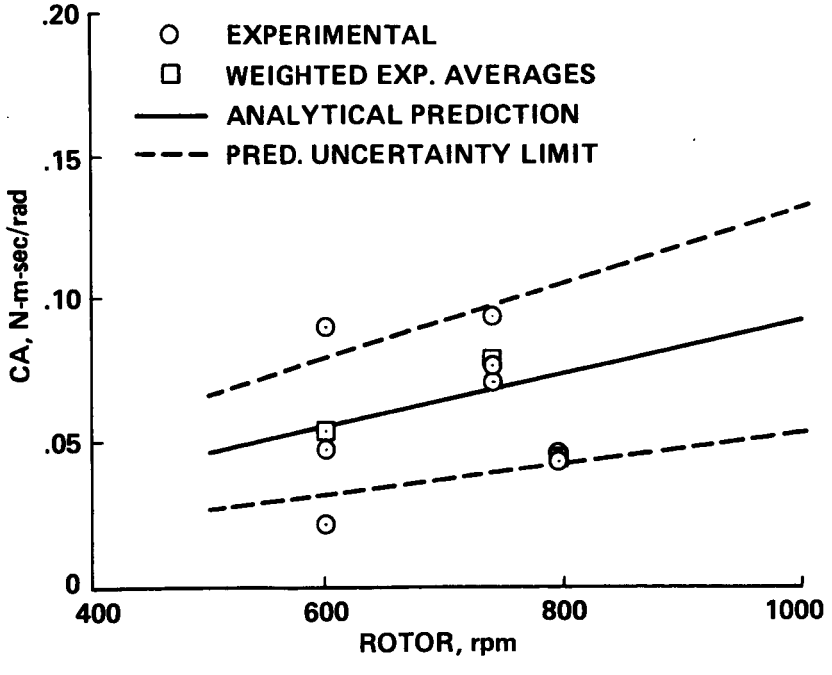

Figure 16.- Free-tip aerodynamic-damping analytical and experimental comparison.

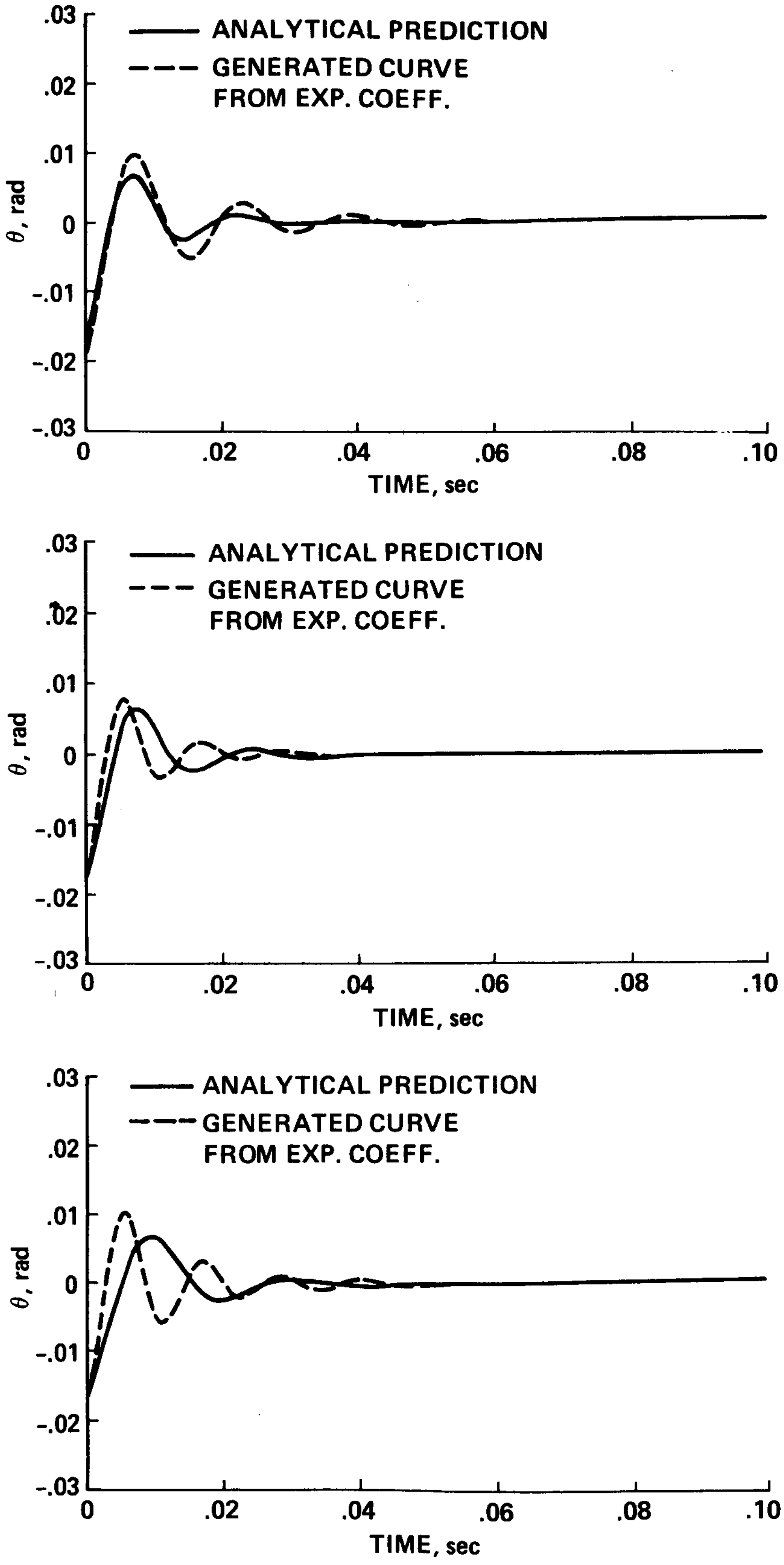

Figure 17.- Analytical and empirically generated transient responses.
(a) Transient-response comparison, 796 rpm. (b) Transient-response comparison, 740 rpm. (c) Transient-response comparison, 600 rpm.

1. Report No.	2. Government Accession No.	3. Recipient's Catalog No.
NASA TM-88250		

4. Title and Subtitle	5. Report Date
AN EXPERIMENTAL INVESTIGATION OF FREE-TIP RESPONSE TO A JET	September 1986
	6. Performing Organization Code
7. Author(s)	8. Performing Organization Report No.
Larry A. Young	A-86234
	10. Work Unit No.
9. Performing Organization Name and Address	
Ames Research Center Moffett Field, CA 94035	11. Contract or Grant No.
	13. Type of Report and Period Covered
12. Sponsoring Agency Name and Address	Technical Memorandum
National Aeronautics and Space Administration Washington, DC 20546	14. Sponsoring Agency Code 505-61-51

15. Supplementary Notes

Point of Contact: Larry A. Young, Ames Research Center, M/S 247-1
Moffett Field, CA 94035 (415) 694-6732 or FTS 464-6732

16. Abstract

The aerodynamic response of passively oscillating tips appended to a model helicopter rotor was investigated during a whirl test. Tip responsiveness was found to meet free-tip rotor requirements. Experimental and analytical estimates of the free-tip aerodynamic spring, mechanical spring, and aerodynamic damping were calculated and compared. The free tips were analytically demonstrated to be operating outside the tip resonant response region at full-scale tip speeds. Further, tip resonance was shown to be independent of tip speed, given the assumption that the tip forcing frequency is linearly dependent upon the rotor rotational speed.

17. Key Words (Suggested by Author(s))	18. Distribution Statement
Free-tip rotor Tip response Aerodynamic spring Aerodynamic damping	Unlimited Subject Category - 02

19. Security Classif. (of this report)	20. Security Classif. (of this page)	21. No. of Pages	22. Price*
Unclassified	Unclassified	56	A04

*For sale by the National Technical Information Service, Springfield, Virginia 22161